

# Composite quasiparticle formation and the low-energy effective Hamiltonians of the one- and two-dimensional Hubbard Model

Junwu Gan and Dung-Hai Lee

*Department of Physics, University of California, Berkeley, CA 94720.*

Per Hedegård

*Ørsted Laboratory, Niels Bohr Institute, University of Copenhagen,  
Universitetsparken 5, DK-2100 Copenhagen Ø, Denmark*

We investigate the effect of hole doping on the strong-coupling Hubbard model at half-filling in spatial dimensions  $D \geq 1$ . We start with an antiferromagnetic mean-field description of the insulating state, and show that doping creates solitons in the antiferromagnetic background. In one dimension, the soliton is topological, spinless, and decoupled from the background antiferromagnetic fluctuations at low energies. In two dimensions and above, the soliton is non-topological, has spin quantum number  $1/2$ , and is strongly coupled to the antiferromagnetic fluctuations. We derive the effective action governing the quasiparticle motion, study the properties of a single carrier, and comment on a possible description at finite concentration.

PACS Numbers: 71.10.Fd, 74.20.Mn, 71.27.+a

## I. INTRODUCTION

Nearly sixty years ago, Peierls first suggested that correlation effects are the cause of the insulating behavior in nickel oxide.<sup>1</sup> Today, we know that NiO is an example of a “Mott insulator” – an insulator that would be metallic by valence counting. The parent compounds of high temperature superconductors, e.g.,  $\text{La}_2\text{CuO}_4$ , are well described as Mott insulators, and have stimulated a renewed interest in the subject.

Mott insulators are generally antiferromagnetic, a feature which makes a mean-field spin-density-wave (SDW) description possible<sup>2</sup>. Although an antiferromagnetic insulator within the SDW description resembles a band insulator, the difference between the two types of insulators is most pronounced when charge carriers are added. Doping a band insulator (say with  $p$ -type dopants) moves the Fermi energy from midgap into the valence band. The hole “pocket” in the valence band is responsible for the conductivity. In a Mott insulator, however, doping creates solitons: localized regions of suppressed antiferromagnetic order in which the hole is confined. The energies of the soliton states lie inside the SDW gap and pin the chemical potential. The soliton propagation is responsible for the conductivity.

The nature of the solitons in Mott insulators depends on the spatial dimensionality. In one dimension (1D), the solitons are topological – they are the anti-phase domain wall.<sup>3,4</sup> They have spin quantum number zero and are decoupled from the spin fluctuations at low energies. As a result of the decoupling, the quasiparticle bandwidth is only weakly renormalized.<sup>4</sup> In  $D \geq 2$ , the solitons are non-topological – they are “bag”-like objects in which the antiferromagnetic order is suppressed consistent with the symmetry of the underlying lattice.<sup>5–7</sup> They carry spin and interact strongly with the low-energy spin fluctuations, significantly reducing the quasiparticle bandwidth.

Both numerical evidence and the behavior of the optical conductivity in the high temperature superconductors are suggestive of the existence of such quasiparticles in two dimensions. Numerical solutions for the single particle Green’s function indicate a single pole and an incoherent background.<sup>8–13</sup> In the high  $T_c$  oxides, the optical conductivity<sup>14</sup> contains two components, a Drude peak and a broad mid-infrared absorption, which are related to the added charge carriers (their spectral weight satisfies the sum rule) and can not be well fit over the entire region assuming conventional quasiparticles. Furthermore, the two components have very different temperature dependence. While the Drude peak is sensitive to temperature (e.g. the width of the Drude peak is  $\approx 2k_B T$ ), the mid-infrared part is not. In fact, the latter survives even in the superconducting state. This type of optical conductivity is, however, what would be expected from solitonic quasiparticles whose conduction is responsible for the Drude peak and whose internal structure generates the mid-infrared absorption. Such behavior is seen in other doped Mott insulators,<sup>15</sup> and systems such as doped Polyacetylene<sup>16</sup> in which solitons are known to exist.

In this paper, we solve the mean-field equations self-consistently to determine the internal structure of the soliton and then examine the motion of the soliton in the antiferromagnetic background. In the mean-field treatment described below, the directional fluctuations of the order parameter are turned off. Consequently, the mean-field solution exhibits long-range order which breaks the lattice translational symmetry. At low energy and long wavelength the important

dynamical degrees of freedom are *a*) the motion of the charged solitons, and *b*) the directional fluctuation of the antiferromagnetic order parameter. These quantum fluctuations restore the symmetry broken at the mean-field level. To obtain an effective action governing these important dynamical processes, we force the antiferromagnetic order parameter to have both solitons (with time-dependent locations) and space-time-dependent directional twists. We then eliminate the electron degrees of freedom corresponding to particle-hole pair excitations.

In one dimension, the soliton in the Hubbard model is intimately related to the structure soliton in doped Polyacetylene.<sup>17</sup> In Polyacetylene, the soliton arises because the ground state of the undoped material breaks a two-fold symmetry of the total electron-phonon Hamiltonian. For the undoped (i.e. half-filled) Hubbard model in 1D, there is no known broken symmetry. The spin-spin correlation decays algebraically.<sup>18</sup> From this point of view it is surprising that there exist finite-size solitons upon doping. The key to the solution of the puzzle is the realization of the very different roles played by the longitudinal (magnitude) and transverse (direction) components of the antiferromagnetic order parameter. A useful picture for the algebraic order in the 1D Hubbard model is the following: Imagine locally (in the sense of both space and time) the order parameter has a well-developed magnitude. However, on a much larger space-time scale, the direction of these local order parameters fluctuates, which destroys the long-range order. In other words, the algebraic antiferromagnetic correlation is due to the power-law decay of the directional correlation between local order parameters, not due to the absence of local moments. In the case of high  $T_c$  oxides (2D system), this picture is supported by experiments.<sup>19</sup> Thus the mean-field longitudinal spin order plays precisely the same role as the Peierls order does in Polyacetylene.

The soliton in 1D is a  $\pi$ -phase-shift domain wall between the two different mean-field ground states. In the absence of doping the soliton is unstable. In fact once we allow the spin direction to fluctuate, the soliton decays into an infinite-width spin twist. Finite-size solitons are stabilized by doping. As will be shown later, after accommodating a hole, a charge soliton remains sharp even when the directional fluctuations are allowed. The resulting action governing the charge and spin dynamics are given by Eqs. (24) and (39). Here we note that due to the fact that the charged solitons are spinless, the two degrees of freedom are decoupled.

In 2D a domain wall is an extended object. Thus one may expect that it is more difficult for doping to stabilize it. For *one hole* in a half-filled Hubbard model with sufficiently big  $U/t$  ( $t$  is the hopping amplitude and  $U$  is the onsite repulsion strength), we find that this expectation is indeed true. In this case we find that the doped charge is accommodated by a localized *non-topological* soliton (or a spin bag). This soliton is the finite  $U$  generalization of a hole in the  $t$ - $J$  model: It has spin quantum number  $1/2$  and its spin direction is constrained to be opposite to the magnetic moment in its absence. Here due to the finiteness of  $U$ , a small amount of double occupation exists, and the size of the soliton depends on  $U/t$ . The effective action describing soliton motion and antiferromagnetic fluctuations is the  $t$ - $J$  model. Due to the coupling to the antiferromagnetic fluctuations, the soliton will be further dressed to form a quasiparticle.

The quasiparticle formation can be simply understood in the string picture by considering the soliton propagation in the antiferromagnetic background.<sup>9,11,20</sup> As the soliton moves, it leaves behind a string of overturned spins which cost antiferromagnetic energy. This energy cost inhibits the motion of the soliton and mimics the effects of a linearly confining potential. The bound state of the soliton in this potential is the quasiparticle.<sup>20</sup> It is important to point out that spin flipping processes in principle can erase the string of frustrated bonds behind the soliton and enable it to escape the potential. If that happens the quasiparticle is no longer well defined. Exact numerical studies of one hole in an antiferromagnet, however, suggest that this does not happen and the quasiparticle picture remains valid. For the 2D Hubbard model with  $t$  and  $U$  chosen in the range relevant to the high- $T_c$  superconductors, the quasiparticle size is about  $3 \sim 5$  lattice spacings.<sup>8-13,21-26</sup> We therefore expect that the qualitative properties of the quasiparticle, such as its quantum numbers, are not changed by the omitted spin flipping processes. However, all quantitative aspects are subject to renormalization. In addition to their effect on the internal structure of the quasiparticle, quantum spin fluctuations have another important effect – they generate coherent propagation of the quasiparticle as a whole. The result is that the quasiparticle primarily hops between neighboring sites within the same sublattice. In the presence of slow time-dependent twisting of the antiferromagnetic order, the quasiparticle spin must follow the direction of the instantaneous local moment. Thus we arrive at the following “surfing model”: Imagine a slowly fluctuating membrane whose normal directions define the local directions of the magnetic moments, then the quasiparticles surf on the membrane but have to keep their spins locally perpendicular to the membrane. This is illustrated in Fig. 1. It is known<sup>27-30</sup> that when a quantum mechanical particle moves on a fluctuating curved surface under the constraint that its spin must be normal to the local surface element, it experiences a Berry phase factor originating from the overlap of its spin states at different space-time points. If the curvature of the surface is nonzero, such a Berry phase cannot be eliminated by a gauge transformation. The effect is analogous to that of a fluctuating magnetic field. This is precisely the origin of the fluctuating gauge field in the effective theory, Eqs. (44) and (45), of the Hubbard (or  $t$ - $J$ ) model.

The layout of the rest of the paper is as follows. In Sec. II, we describe the path integral formalism for the Hubbard model. In Sec. III, we apply this formalism to the 1D Hubbard model, show how the standard results are reproduced,

and develop the analogy with Polyacetalene. In Sec. IV, we apply the formalism to the 2D Hubbard model, discuss the connection with the spin-bag model proposed by Schrieffer, Wen, and Zhang<sup>5</sup>, examine the quasiparticle formation, and derive an effective action. In Sec. V, we give a conclusion and a summary of our results.

## II. PATH INTEGRAL FORMALISM

The Hamiltonian of the Hubbard model is,

$$H = -t \sum_{\langle i,j \rangle, \sigma} (c_{i\sigma}^\dagger c_{j\sigma} + c_{j\sigma}^\dagger c_{i\sigma}) + U \sum_i n_{i\uparrow} n_{i\downarrow}, \quad (1)$$

where  $c_{i\sigma}^\dagger$  is the electron creation operator and  $n_{i\sigma} = c_{i\sigma}^\dagger c_{i\sigma}$ . The summation over  $\langle i, j \rangle$  only includes the nearest neighbor links. The partition function is given by

$$Z = \int \mathcal{D}[c, \bar{c}] \exp \left\{ - \int_0^\beta d\tau \left[ \sum_{i,\sigma} \bar{c}_{i\sigma} (\partial_\tau - \mu) c_{i\sigma} + H \right] \right\}, \quad (2)$$

where  $\mu$  is the chemical potential.

The usual way to proceed from here is to factorize the Hubbard interaction via a Hubbard-Stratonovich transformation. There are many ways to factorize the Hubbard interaction, and in principle they are all equivalent. However, if one does not perform the functional integral over the Hubbard-Stratonovich field exactly, in particular if one only integrates over the long-wavelength and low-frequency components of the auxiliary field, then different decoupling scheme gives different results. The latter is a well known phenomenon. For example in the mean-field theory (i.e. one only keeps the  $\vec{q} = 0, \omega = 0$  components of the Hubbard-Stratonovich field) it is crucial to find the ‘‘right’’ decoupling scheme, or equivalently the right order parameter. The situation can be even worse. In some cases the low- $\vec{q}$  and low- $\omega$  components of the Hubbard-Stratonovich fields associated with different decoupling scheme captures different aspect of the low-energy physics. When that happens one has to include all relevant auxiliary fields in the effective action. For a prior example of such multi-auxiliary-field treatment, the reader is referred to Finkelstein’s derivation of the non-linear  $\sigma$  model for the correlated disorder transport problem.<sup>31</sup>

For the Hubbard model near half-filling, we expect that the important charge fluctuations are near momentum  $\vec{q} = 0$ , while the important spin fluctuations in 2D are around  $\vec{q} = (\pi, \pi)$ . In the following we shall use  $\{A\}_{\vec{q}_0 + \vec{q}}$  to denote the slow  $A$ -modes around the modulation wave vector  $\vec{q}_0$  and implicitly impose the condition  $|\vec{q}| < \pi$ . Inspired by the above understanding the Hubbard interaction factorizes into the following fluctuation channels,

$$\begin{aligned} \sum_j \bar{c}_{j\uparrow} c_{j\uparrow} \bar{c}_{j\downarrow} c_{j\downarrow} &\simeq \sum_{|\vec{q}| < \pi} \left[ \frac{1}{4} \{ \bar{c}_\uparrow c_\uparrow + \bar{c}_\downarrow c_\downarrow \}_{\vec{q}} \{ \bar{c}_\uparrow c_\uparrow + \bar{c}_\downarrow c_\downarrow \}_{-\vec{q}} - \{ \bar{c}_\uparrow c_\downarrow \}_{\vec{\pi} + \vec{q}} \{ \bar{c}_\downarrow c_\uparrow \}_{-\vec{\pi} - \vec{q}} \right. \\ &\quad \left. - \frac{1}{4} \{ \bar{c}_\uparrow c_\uparrow - \bar{c}_\downarrow c_\downarrow \}_{\vec{\pi} + \vec{q}} \{ \bar{c}_\uparrow c_\uparrow - \bar{c}_\downarrow c_\downarrow \}_{-\vec{\pi} - \vec{q}} \right]. \end{aligned} \quad (3)$$

where  $\vec{\pi} = (\pi, \pi)$ . Note that the factor 1/4 in front of the first and third terms on the right hand side of (3) is obtained by omitting the following two terms in the factorization:  $(1/4) \{ \bar{c}_\uparrow c_\uparrow - \bar{c}_\downarrow c_\downarrow \}_{\vec{q}} \{ \bar{c}_\uparrow c_\uparrow - \bar{c}_\downarrow c_\downarrow \}_{-\vec{q}}$  and  $(1/4) \{ \bar{c}_\uparrow c_\uparrow + \bar{c}_\downarrow c_\downarrow \}_{\vec{\pi} + \vec{q}} \{ \bar{c}_\uparrow c_\uparrow + \bar{c}_\downarrow c_\downarrow \}_{-\vec{\pi} - \vec{q}}$ . In the above we have explicitly omitted the Cooper channel. The necessary Hubbard-Stratonovich decoupling thus includes

$$\begin{aligned} U \sum_j \bar{c}_{j\uparrow} c_{j\uparrow} \bar{c}_{j\downarrow} c_{j\downarrow} &\rightarrow \sum_{|\vec{q}| < \pi} \left\{ i \Delta_c(\vec{q}) \{ \bar{c}_\uparrow c_\uparrow + \bar{c}_\downarrow c_\downarrow \}_{-\vec{q}} + \frac{1}{U} \Delta_c(\vec{q}) \Delta_c(-\vec{q}) \right. \\ &\quad + \Delta_z(\vec{\pi} + \vec{q}) \{ \bar{c}_\uparrow c_\uparrow - \bar{c}_\downarrow c_\downarrow \}_{-\vec{\pi} - \vec{q}} + \frac{1}{U} \Delta_z(\vec{\pi} + \vec{q}) \Delta_z(-\vec{\pi} - \vec{q}) \\ &\quad \left. + \bar{\Delta}_+(\vec{\pi} + \vec{q}) \{ \bar{c}_\uparrow c_\downarrow \}_{\vec{\pi} + \vec{q}} + \{ \bar{c}_\downarrow c_\uparrow \}_{\vec{\pi} + \vec{q}} \Delta_+(\vec{\pi} + \vec{q}) + \frac{1}{U} |\Delta_+(\vec{\pi} + \vec{q})|^2 \right\}. \end{aligned} \quad (4)$$

In coordinate-space we have

$$\begin{aligned}
U \sum_j \bar{c}_{j\uparrow} c_{j\uparrow} \bar{c}_{j\downarrow} c_{j\downarrow} &\rightarrow \sum_j \left\{ i\Delta_c(j) (\bar{c}_{j\uparrow} c_{j\uparrow} + \bar{c}_{j\downarrow} c_{j\downarrow}) + \frac{1}{U} \Delta_c^2(j) \right. \\
&+ (-1)^j \Delta_z(j) (\bar{c}_{j\uparrow} c_{j\uparrow} - \bar{c}_{j\downarrow} c_{j\downarrow}) + \frac{1}{U} \Delta_z^2(j) \\
&\left. + (-1)^j [\bar{\Delta}_+(j) \bar{c}_{j\uparrow} c_{j\downarrow} + \bar{c}_{j\downarrow} c_{j\uparrow} \Delta_+(j)] + \frac{1}{U} |\Delta_+(j)|^2 \right\}. \tag{5}
\end{aligned}$$

In the above, we have explicitly pulled out the staggering factor from  $\Delta_z(j)$  and  $\Delta_+(j)$ . Therefore, all the remaining variables  $\Delta_c(j)$ ,  $\Delta_z(j)$  and  $\Delta_+(j)$  are smooth fields. In 2D, each lattice site is labelled by two integers,  $j = (j_x, j_y)$ , in the unit of lattice constant, and the staggering factor denotes  $(-1)^j = (-1)^{j_x + j_y}$ .

Combining Eqs. (1) to (5), the partition function can be approximated as,

$$Z \approx \int \mathcal{D}[c, \bar{c}, \Delta_c, \Delta_z, \Delta_+, \bar{\Delta}_+] \exp \left\{ - \int_0^\beta d\tau \left[ \sum_{j,\sigma} \bar{c}_{j\sigma} (\partial_\tau - \mu) c_{j\sigma} + H' \right] \right\}, \tag{6}$$

$$\begin{aligned}
H' &= -t \sum_{\langle i,j \rangle, \sigma} (\bar{c}_{i\sigma} c_{j\sigma} + h.c.) + \frac{1}{U} \sum_j \{ [\Delta_c(j)]^2 + [\Delta_z(j)]^2 + |\Delta_+(j)|^2 \} \\
&+ \sum_{j,\alpha\beta} \bar{c}_{j\alpha} \left\{ i\Delta_c(j) + (-1)^j \left[ \Delta_z(j) \sigma_z + \frac{1}{2} \bar{\Delta}_+(j) (\sigma_x + i\sigma_y) + \frac{1}{2} \Delta_+(j) (\sigma_x - i\sigma_y) \right] \right\}_{\alpha\beta} c_{j\beta}. \tag{7}
\end{aligned}$$

The fact that only smooth configurations of  $\Delta_c(j)$ ,  $\Delta_z(j)$  and  $\Delta_+(j)$  are included in the path integral ensures that there is no overcounting.

To emphasize the SU(2) symmetry we group  $\Delta_z(j)$  and  $\Delta_+(j)$  together and write them as

$$\Delta_z(j) \sigma_z + \frac{1}{2} \bar{\Delta}_+(j) (\sigma_x + i\sigma_y) + \frac{1}{2} \Delta_+(j) (\sigma_x - i\sigma_y) = \Delta_s(j) g^+(j) \sigma_z g(j). \tag{8}$$

Here  $\Delta_s(j)$  is a real scalar field representing the longitudinal component of the local moment, while  $g(j)$  is an SU(2) matrix encoding the transverse components of the local moment. We emphasize that both  $\Delta_s(j)$  and  $g(j)$  are smooth functions of space and time.

Let us now perform a space-time-dependent local gauge transformation to absorb the  $g$  and  $g^+$  in Eq.(8).

$$\bar{c}'_i = \bar{c}_i g^+(i), \quad \text{with } \bar{c}_i = (\bar{c}_{i\uparrow}, \bar{c}_{i\downarrow}). \tag{9}$$

We then rewrite everything in terms of the new variables. A straightforward manipulation shows that<sup>32</sup>

$$Z = \int \mathcal{D}[c, \bar{c}, \Delta_c, \Delta_s, g] \exp \left\{ - \int_0^\beta d\tau \mathcal{L} \right\}, \tag{10}$$

$$\begin{aligned}
\mathcal{L} &= \sum_j \bar{c}_j [\partial_\tau + g(j) \partial_\tau g^+(j) + (-1)^j \Delta_s(j) \sigma_z + i\Delta_c(j) - \mu] c_j \\
&- t \sum_{\langle i,j \rangle} [\bar{c}_i g(i) g^+(j) c_j + h.c.] + \frac{1}{U} \sum_j [\Delta_c^2(j) + \Delta_s^2(j)]. \tag{11}
\end{aligned}$$

In the above we have omitted the primes on the Grassmann variables. Our subsequent treatments of the path integral (11) involve a saddle point analysis followed by expansions that include small fluctuations around the latter. In specific our saddle analysis assumes time-independent (but spatially dependent) fields given by

$$\Delta_c(\tau, j) = -i\Delta_c^{(0)}(j), \tag{12}$$

$$\Delta_s(\tau, j) = \Delta_s^{(0)}(j), \tag{13}$$

$$g(\tau, j) = g_0(j), \tag{14}$$

and the corresponding saddle point equations are

$$\Delta_c^{(0)}(j) = \frac{U}{2} \langle n_j \rangle, \tag{15}$$

$$\Delta_s^{(0)}(j) \text{Tr} [g_0^+(j) \sigma_z g_0(j) \sigma_\alpha] = -U (-1)^j \langle c_{j\sigma}^\dagger \sigma_\alpha c_j \rangle, \quad \alpha = x, y, z. \tag{16}$$

In the above  $n_j \equiv \sum_\sigma c_{j\sigma}^\dagger c_{j\sigma}$ . This analysis is equivalent to the Hartree-Fock solution. It is also equivalent to the variational solution constructed using a Slater determinant as the trial wave function.

### III. THE ONE-DIMENSIONAL HUBBARD MODEL REVISITED

The purpose of this section is to demonstrate that our approach reproduces the well known results in 1D. Hopefully it will strengthen the readers' confidence (as well as ours) when it is applied to 2D.

#### A. 1D Hubbard model at half-filling: the non-linear $\sigma$ model

To warm up, let us first consider the 1D Hubbard model at half-filling (i.e. with on average one electron per site). It is known that for arbitrary repulsion, the half-filled Hubbard model in 1D is a charge insulator, and the only low-energy excitations are spin in nature. Here we derive the effective theory for such spin excitations.

We first find the saddle point solution in the form of Eqs.(12)–(14). The result is

$$\Delta_c(j) = -i\Delta_c^{(0)}, \quad \Delta_s(j) = \Delta_s^{(0)}, \quad g(j) = 1. \quad (17)$$

The corresponding saddle point(or mean field) Hamiltonian is

$$H_{mf} = -t \sum_{\langle i,j \rangle} (c_i^\dagger c_j + h.c.) + \sum_i c_i^\dagger \left[ (-1)^i \Delta_s^{(0)} \sigma_z - \tilde{\mu} \right] c_i + \frac{1}{U} \left[ (\Delta_s^{(0)})^2 - (\Delta_c^{(0)})^2 \right] \mathcal{N}, \quad (18)$$

where  $\mathcal{N}$  is the number of lattice sites and

$$\tilde{\mu} = \mu - \Delta_c^{(0)}. \quad (19)$$

This Hamiltonian can be easily diagonalized. At half-filling  $\tilde{\mu} = 0$  and  $\Delta_s^{(0)}$  satisfies<sup>33</sup>

$$\frac{2}{U} = \int_0^{2\pi} \frac{dk}{2\pi} \frac{1}{\sqrt{(2t \cos k)^2 + (\Delta_s^{(0)})^2}}. \quad (20)$$

For  $U/t = 8/3, 4,$  and  $8,$  the solutions to Eq.(20) give  $\Delta_s^{(0)} \approx 0.726t, 1.539t,$  and  $3.754t$  respectively. The solution describes a long-range ordered antiferromagnets with the local moment  $m_0 = 0.272, 0.384$  and  $0.469$  respectively. The mean-field electronic spectrum has a gap separating an empty conduction band from a full valence one.

To study the low-energy excitations, we include fluctuations in  $\Delta_c(j), \Delta_s(j)$  and  $g(j)$  around their saddle point values, and integrate out  $c$  and  $\bar{c}$ . Since the action is quadratic in the fermion variables after Hubbard-Stratonovich factorization, the integration produces a fermion determinant. It turns out that both  $\Delta_c(j)$  and  $\Delta_s(j)$  fluctuations are gapful, thus can be safely ignored at low energies. We expand the fermion determinant to quadratic order in  $g\partial_\mu g^+$  to obtain (the details are supplied in appendix B)

$$\mathcal{L}_{\text{eff}} = \sum_i \langle S_i^z \rangle \text{Tr} [\sigma_z g(i) \partial_\tau g^+(i)] + \frac{\rho_s}{2} \int dx \sum_{\mu=\nu_F \tau, x} [\text{Tr} (\partial_\mu g \partial_\mu g^+) + \text{Tr} (\sigma_z g \partial_\mu g^+ \sigma_z g \partial_\mu g^+)]. \quad (21)$$

In the above,  $\langle S_i^z \rangle = \langle c_i^\dagger \sigma_z c_i \rangle / 2 = (-1)^i m_0$  is the mean field magnetization, and  $\rho_s$  is the spin stiffness given by Eq. (B26). The spin wave velocity turns out to be the same as the bare Fermi velocity. The second term in (21) is the well known non-linear  $\sigma$  model written in terms of the SU(2) matrix  $g(i)$ . Using  $\vec{n} \cdot \vec{\sigma} = g^+ \sigma_z g$ , one can easily verify that

$$(\partial_\mu \vec{n})^2 = \text{Tr} (\partial_\mu g \partial_\mu g^+) + \text{Tr} (\sigma_z \partial_\mu g^+ \sigma_z g \partial_\mu g^+).$$

The first term of (21) represents a Berry phase. To see this, we express

$$g = \begin{pmatrix} z_1^* & z_2^* \\ -z_2 & z_1 \end{pmatrix}, \quad (22)$$

where  $\sum_\sigma z_\sigma^* z_\sigma = 1$ . In terms of  $z^* = (z_1^*, z_2^*)$ ,  $\vec{n} = z^* \vec{\sigma} z$ . It is straightforward to show that

$$\begin{aligned} m_0 \sum_i (-1)^i \text{Tr} [\sigma_z g(i) \partial_\tau g^+(i)] &= 2m_0 \sum_i (-1)^i z^*(i) \partial_\tau z(i) \\ &= i \frac{\theta}{2\pi} \int dx \partial_x \vec{n} \cdot (\vec{n} \times \partial_\tau \vec{n}), \quad \theta = 2\pi m_0. \end{aligned} \quad (23)$$

While our approximate calculations do yield the right form for the effective action, it makes a serious mistake. It is well known that the  $\theta$  in the effective action is quantized to have the value  $\pi$ .<sup>18</sup> Our approximate calculation gives a  $\theta$  that depends on the magnitude of the local moment. It is also known that the low-energy behavior of the non-linear sigma model critically depends on the value of  $\theta$ .<sup>34,35</sup> In particular, the spin excitation spectrum is gapless only when  $\theta = (2n + 1)\pi$ . Since  $m_0 \leq 1/2$ , we would conclude that except for the case of  $U = \infty$  (in that case  $m_0 \rightarrow 1/2$ ) the spin spectrum is always gapful. This is, of course, incorrect. Then what is wrong with our derivation?

The answer relies on the fact that the value of  $\theta$  reveals a symmetry of the problem. The original 1D Hubbard model is invariant under the translation by one lattice spacing. Since it is known that the ground state of the model preserves this symmetry, it better be true that any low energy effective theory is revealing it. This is not so in Eq. (23) unless  $\theta = \text{integer} \times \pi$ . Indeed, as  $x \rightarrow x + a$ ,  $m_0 \rightarrow -m_0$  which invert the sign of  $\theta$ . Since  $\frac{1}{2\pi} \int dx \partial_x \vec{n} \cdot (\vec{n} \times \partial_\tau \vec{n})$  is an integer, the latter is a symmetry only when  $\theta$  is an integer multiples of  $\pi$ .

Thus if we did the calculation exactly,  $\theta$  should turn out to be  $\pi$ . This has been shown to be the case recently by Nagaosa and Oshikawa<sup>36</sup>. The point is that approximations are not allowed in extracting quantized quantities. To proceed, we offer the following symmetry based arguments to fix the value of  $\theta$ .<sup>18</sup> Since from translational symmetry  $\theta = \text{integer} \times \pi$ , our job is only to determine which integer. For this purpose we recall that as a function of  $U/t$  the half-filled Hubbard model experiences no phase transition. Thus it is sufficient for us to determine  $\theta$  in the  $U/t \rightarrow \infty$  limit. Since in the latter limit the leading order result becomes exact, and since  $\theta$  remains quantized as we vary  $U/t$ , we can deduce its value exactly. As  $U/t \rightarrow \infty$ ,  $m_0 \rightarrow 1/2$  and  $\theta \rightarrow \pi$ , thus we conclude that the exact value of  $\theta$  in Eq. (23) is  $\pi$ .

Summarizing the above discussions, we have arrived at the following low-energy effective theory for the 1D Hubbard model at half-filling:

$$S_{\text{eff}} = \int_0^\beta d\tau \int dx \left\{ \frac{i}{2} \partial_x \vec{n} \cdot (\vec{n} \times \partial_\tau \vec{n}) + \frac{\rho_s}{2} \left[ \frac{1}{v_F^2} (\partial_\tau \vec{n})^2 + (\partial_x \vec{n})^2 \right] \right\}. \quad (24)$$

The consequence of this action is that transverse fluctuations destroy the long-range order in the saddle point solution. The result is a quasi-long-range antiferromagnetically correlated state in which the correlation between local Néel order decays as the inverse of distance.

## B. The charge and spin excitations away from half-filling

In this section, we shall show that away from half-filling the elementary excitations of the 1D Hubbard model are holons and spinons. In addition we shall demonstrate the similarities between the holon and the soliton in Polyacetylene.

Our starting point is the saddle-point solution of Eq. (11). Naively one might take the half-filled solution and take out an electron from the valence band. This is dangerous since one overlooks the effect of doping on the saddle-point solution. For example in the presence of a static hole, we do not expect the saddle point solution to have spatially uniform spin and charge density. This is because the spin and charge densities are self-consistently determined by the occupation of the electronic states. Around the hole, the electron density is reduced so that the magnitude of  $\langle S_i^z \rangle$  must also be reduced. Motivated by the above considerations we look for a self-consistent solution of the following form:

$$\Delta_c(j) = -i\Delta_c^{(0)}(j), \quad \Delta_s(j) = \Delta_s^{(0)}(j), \quad g(j) = 1. \quad (25)$$

The saddle point Hamiltonian is

$$H_{mf} = -t \sum_{\langle i,j \rangle} \left( c_i^\dagger c_j + h.c. \right) + \sum_j c_j^\dagger \left[ \Delta_c^{(0)}(j) - \mu + (-1)^j \Delta_s^{(0)}(j) \sigma_z \right] c_j + \frac{1}{U} \sum_j \left\{ \left[ \Delta_s^{(0)}(j) \right]^2 - \left[ \Delta_c^{(0)}(j) \right]^2 \right\}. \quad (26)$$

In Appendix A, we show that the continuum version of Eq. (26) is very similar to the corresponding continuum Hamiltonian for Polyacetylene.<sup>37</sup> The saddle point equations are

$$\Delta_s^{(0)}(i) = -(-1)^i \frac{U}{2} \left[ \langle c_{i\uparrow}^\dagger c_{i\uparrow} \rangle - \langle c_{i\downarrow}^\dagger c_{i\downarrow} \rangle \right], \quad (27)$$

$$\Delta_c^{(0)}(i) = \frac{U}{2} \left[ \langle c_{i\uparrow}^\dagger c_{i\uparrow} \rangle + \langle c_{i\downarrow}^\dagger c_{i\downarrow} \rangle \right]. \quad (28)$$

We solve the above equations numerically in a finite chain of 100 sites with 99 electrons under the open boundary condition. Armed with the experience from Polyacetylene, we choose the starting point of the self-consistent iteration to be

$$\Delta_s^{(0)}(i) = \Delta_s^{(0)} \tanh\left(\frac{i-x_0}{\xi}\right), \quad \Delta_c^{(0)}(i) = \frac{U}{2}, \quad (29)$$

where  $x_0$  and  $\xi$  are two arbitrary parameters and  $\Delta_s^{(0)}$  is the solution at half filling. It turns out that for small  $U/t$ , the self-consistent iteration preserves  $x_0$ . The resulting self-consistent saddle point solution suggests that  $x_0$  does not necessarily center at a high symmetry position (such as a lattice site or the mid-point of a lattice bond). To ensure that the 100-site chain is sufficiently long,<sup>38</sup> we have checked that the difference between the values of  $\Delta_s^{(0)}$  under periodic and open boundary conditions at half filling only shows up at the fourth significant figures. For  $U/t = 8/3$  the saddle point solution and the associated spin and charge profiles with the kink centered at the middle of a lattice link are shown in Fig. 2 and Fig. 6 respectively.

We notice that the boundary effects die off a few lattice spacings away from the two ends of the chain.<sup>38</sup> The ground state energy at the saddle point is  $-0.196t (-0.269\Delta_s^{(0)})$  for  $U/t = 8/3$ , where the reference energy is chosen to be the energy of the “doped semiconductor state” obtained by removing one electron from the top of the valence band of the half-filled self-consistent band structure under open boundary condition. For other values of  $U/t$  ratios, the energies of the saddle point solutions with  $x_0$  situated at the mid-point of a bond are  $-0.242t (-0.260\Delta_s^{(0)})$  for  $U/t = 3$ ,  $-0.366t (-0.238\Delta_s^{(0)})$  for  $U/t = 4$ , and  $-0.643t (-0.171\Delta_s^{(0)})$  for  $U/t = 8$ .

The one-electron spectrum for  $U/t = 8/3$  is shown in Fig. 3. As in Polyacetylene, there are two midgap states. These states have opposite spin quantum numbers, and are almost degenerate. Their wave functions are shown in Fig. 4. All energy levels below these two states are occupied. The spin and charge densities of the saddle point solution can be fitted to simple analytic functions. The least-square fitting gives, for  $U/t = 8/3$ ,

$$(-1)^i \langle S_i^z \rangle = \frac{\Delta_s^{(0)}}{U} \tanh\left(\frac{i-x_0}{\xi_s}\right), \quad \xi_s = 2.978, \quad (30)$$

$$\langle n_i \rangle = 1 - \frac{1}{2\xi_c \cosh^2\left(\frac{i-x_0}{\xi_c}\right)}, \quad \xi_c = 3.209. \quad (31)$$

The quality of the fitting is demonstrated in Fig. 5. In principle, we still have to show that we have allowed sufficient variational degrees of freedom in our mean-field ansatz Eq.(25). Here we skip this issue by referring the reader to the similar situations in Polyacetylene where the the soliton stability was proven.<sup>16</sup>

Intuitively one expects that the kink energy reaches optimum if the center of the kink is located at high symmetry positions of the chain. It turns out that for e.g.  $U/t = 8/3$  the kink energy has no measurable dependence on its position! This is, of course, what one expects based on the continuum Hamiltonian we derive in Appendix A. The validity of the continuum approximation is that the self-consistent spin and charge densities have smooth spatial variations. This requirement will eventually be violated when  $U/t \gg 1$ , in which case the kink is a very localized object. In the latter case the center of the kink becomes a crucial parameter, not only does it affect the energetics but it also determines whether self-consistency can be reached at all. Indeed, we have found that for large  $U/t$  the only possible self-consistent kink solution is a kink centered at the mid-point of a bond.

The static kink solution discussed above represents a snap shot of the charged quasiparticle of the 1D Hubbard model. If the time scale associated with the motion of the quasiparticle is long compared with the inverse excitation gap of the soliton band structure, to a good approximation we can regard it as a rigid boost of the static soliton discussed above. In that limit, in order to determine the quantum numbers of a moving soliton it is sufficient to study the corresponding quantities assuming the soliton is at rest. In the following we shall assume such an adiabatic picture. Let us first determine the charge of a kink. Since we are interested in the case where a continuum description is possible, we shall concentrate on the case of  $U/t = 8/3$ . Moreover we shall assume that the center of the soliton is situated at the center of a bond. In Fig. 5 we show the change in site occupation number due to the presence of a kink. From Eq. (31) we deduce that

$$\sum_i \langle \delta n_i \rangle \simeq - \int_{-\infty}^{\infty} dx \frac{1}{2\xi_c \cosh^2\left(\frac{x-x_0}{\xi_c}\right)} = -1. \quad (32)$$

Therefore, the kink carries charge  $e$ .

Now we determine the total  $S^z$  associated with a kink. This is sufficient for the purpose of later discussions because it turns out that  $S^z$  plays the role of coupling constant in the residual gauge coupling between the soliton current

and the fluctuating antiferromagnetic background (see later). The total  $\langle S^z \rangle$  associated with a kink is given by,  $\langle S^z \rangle = \sum_i \langle S_{\text{pair}}^z(i) \rangle$ , where  $\langle S_{\text{pair}}^z(i) \rangle \equiv \langle S^z(i) + S^z(i+1) \rangle / 2$ . In Fig. 7 we show the  $\langle S_{\text{pair}}^z(i) \rangle$  profile, where we see that the only nonzero  $\langle S_{\text{pair}}^z(i) \rangle$  appears near the kink. (The zigzag pattern near the chain ends is caused by the boundary and it is not shown in the figure.) Had we plotted the same quantity for the half-filled case we would have found zero everywhere except near the ends of the chain. From Fig. 7, It is clear that by summing up all  $\langle S_{\text{pair}}^z(i) \rangle$  we get zero.

Thus on a scale larger than the size (determined by the larger one between  $\xi_c$  and  $\xi_s$ ) of the kink we can regard it as a point object carrying charge  $e$  and zero  $S^z$ . These quantum numbers are consistent with those of the holon in the 1D Hubbard model.

Next we turn to the neutral spin excitations. In the presence of the longitudinal spin order one naturally expect the low-lying spin excitations to be described by the smooth space-time fluctuating  $g(\tau, i)$ . However, is that all? For instance can we have a neutral spin excitations with a sharp kink form in  $\Delta_s^{(0)}(i)$ ? In the following we show that the answer is no. Specifically, we shall start from the solution corresponding to a charged soliton and show that if the missing electron is put back into the system the soliton decays into a smooth spin twist. For this purpose, it suffices to find a path connecting the configurations corresponding to the kink and the smooth twist, and show that the energy continuously decreases along the path. Considering Eqs. (7) and (8), the path we found is,

$$\begin{aligned} \Delta_c^{(0)}(i) + (-1)^i \Delta_s^{(0)}(i) g^+(i) \sigma_z g(i) &= 1 - \frac{1 - \lambda}{2\xi_c \cosh^2\left(\frac{i-x_0}{\xi_c}\right)} \\ &+ (-1)^i \Delta_s^{(0)} \left[ \tanh\left(\frac{i-x_0}{\xi_s}\right) \sigma_z + \frac{\lambda}{\cosh\left(\frac{i-x_0}{\xi_s}\right)} \sigma_x \right]. \end{aligned} \quad (33)$$

The first segment of the path is given by increasing  $\lambda$  from zero to one while keeping  $\xi_c$  and  $\xi_s$  fixed. We note that when  $\lambda = 1$ , the spin order profile given by Eq. (33) becomes a twist of the size  $\xi_s$ . The second part of the path is to increase  $\xi_s$  while fixing  $\lambda = 1$ . Again we choose a chain of 100 sites with  $U/t = 8/3$  and  $x_0$  situated at the center of a bond for the demonstration. To obtain the electron wave functions along the path we modify the Hamiltonian (26), by replacing the onsite potential term with the right hand side of Eq. (33). We diagonalize this Hamiltonian to construct the wave function by filling 100 electrons in the lowest 100 energy levels. Then we obtain the variational energy by calculating the expectation value of the full Hubbard Hamiltonian. The result is shown in Fig. 8, where the reference energy is chosen to be the energy expectation of the half-filled mean-field state. In the left panel, the energy is shown as the function of  $\lambda$  while fixing  $\xi_s = 2.978$  and  $\xi_c = 3.209$ . We see that the kink is unstable once an additional electron is introduced. This is not difficult to understand if we recall the physics of Jahn-Teller effect. The two nearly degenerate midgap states are empty in the case of charged soliton. If the missing electron is put back, it is energetically favorable to split the two midgap levels and occupy the lower level. The off-diagonal  $\sigma_x$  part in Eq. (33) precisely provides matrix element between these two states and consequently split them. In the right panel of Fig. 8, the variational energy is shown as a function of the twist size  $\xi_s$  while fixing  $\lambda = 1$ . The twist given by Eq. (33) with  $\lambda = 1$  further decays to an infinitely smooth one, as illustrated in Fig. 9. In fact, the twist is just a spinon.<sup>39</sup>

### C. Effective theory

In the above discussions the saddle point solution for doped 1D Hubbard model consists of static and localized solitons (each accommodating one hole) separating the otherwise perfectly ordered antiferromagnetic domains. Ignored in this mean-field theory are the smooth space-time variation of the direction of the order parameter, and the propagation the soliton configurations. In general it is not clear that the saddle point solution in the presence of  $N$  holes is  $N$  separate solitons (for example, it is important to compare the mean-field energies associated with, say, a phase-separated solution with that of  $N$  equally spaced solitons). In the rest of this section we will assume that the individual soliton remains stable against finite doping. Under that assumption we will show that the low-energy theory is precisely the effective theory for the Hubbard model obtained via non-Abelian bosonization (see Appendix B).

We now briefly describe the derivation of the effective action, and leave the details in Appendix B. The basic strategy is to allow the solitons to have time-dependent locations, and twist the spin directions in a space-time dependent way. Then we evaluate the cost in action due to such distortions.

At the length scale longer than the kink size  $\xi_s$ , the kink (30) can be simply viewed as a point at which the longitudinal spin order parameter  $\Delta_s(i)$  flips its sign. Consequently at a given site the sign of  $\Delta_s(i)$  has changed as many times as the number of holons to its left:



$$\Delta_s(x) \simeq \Delta_s^{(0)} \cos \left[ \pi \int_0^x dy n(y) \right], \quad 0 \leq x \leq L, \quad (34)$$

where

$$n(y) = \sum_{i=1}^{N_h} \delta(y - x_i), \quad (35)$$

is the holon density. At low energy and long wavelength we expect the holon density to be its average value  $n_h$  plus small perturbations:  $n(x) = n_h + \delta n(x)$ . The spin order profile in the finite doping becomes, upon replacing the lattice site  $j$  with the continuum coordinate  $x$ ,

$$(-1)^j \Delta_s(j) \rightarrow \Delta_s^{(0)} \cos [2k_F x + \Phi(x)], \quad (36)$$

$$\Phi(x) = -\pi \int_0^x dy \delta n(y). \quad (37)$$

where  $k_F = \pi(1 - n_h)/2$ . Furthermore, the phase  $\Phi(x)$  satisfies the following density-phase conjugation relation:

$$\frac{\partial \Phi(x)}{\partial x} = -\pi \delta n(x). \quad (38)$$

Substituting Eq. (36) into Eq. (11), and integrating out  $c$  and  $\bar{c}$ , we derive the desired low-energy effective theory in the case of finite doping. The charge part is given by a free boson theory

$$S_{\text{eff}}^{(c)} = \frac{\rho_c}{2} \int_0^\beta d\tau \int dx \left[ \frac{1}{v_c^2} (\partial_\tau \Phi)^2 + (\partial_x \Phi)^2 \right], \quad (39)$$

where  $\rho_c$  and  $v_c$  are the charge stiffness and velocity, given by Eqs. (B29) and (B30). The spin part is still given by Eq. (24). Both  $\rho_c$  and  $v_c$  are different from  $\rho_s$  and  $v_F$ . The detailed calculation is included in Appendix B, (also see Reference 36.)

As noted by Lee from the Bethe Ansatz solution<sup>4</sup>, the Fermi velocity in the low-energy effective action is not much different from the bare one of the non-interacting case. This is consistent with the fact that in Appendix B the integral in Eq. (B26) is independent of  $\Delta_s^{(0)}$ . We note that the parameters in the effective action are subject to the renormalizations due to short distance fluctuations which are simply dropped when we take the continuum limit in Appendix B. However, as the order of magnitude is concerned, the results are reliable. This is in sharp contrast to the situation in two dimensions where the effective Fermi velocity is renormalized down to the order of  $J(\sim t^2/U)$ , as we shall see below.

#### IV. THE HUBBARD MODEL IN TWO DIMENSIONS

Since the discovery of the high temperature superconductors, Anderson<sup>40</sup> has been suggesting that the one-band Hubbard model in two dimensions (or the closely related  $t$ - $J$  model<sup>41</sup>) captures the essential physics of the CuO<sub>2</sub> plane in the cuprate superconductors. Ever since then, the properties of 2D Hubbard model (on square lattice in particular) has been a focus of investigations. An important parameter for the cuprates is the doping level. For example, within a class of compounds, the samples with the highest  $T_c$  usually have doping level around 15%. In terms of the Hubbard model it means that the averaged site occupation number is around 0.85. As in one dimension the starting point of our discussion is the half-filled Hubbard model.

By now it is a common consensus that at half-filling, the Hubbard model describes an ordered antiferromagnetic Mott insulator and the long wavelength effective theory is a 2+1 D non-linear  $\sigma$  model<sup>42</sup>. The derivation of the latter from the Hubbard model proceeds in the same way as in one dimension except that the Berry phase term is canceled out in two dimensions.<sup>43</sup> The antiferromagnetic order present in the half-filled 2D Hubbard model reflects the fact that the non-linear  $\sigma$  model can be ordered in 2+1 dimensions.

An important question is how to proceed when the antiferromagnet is doped. In the conventional approach, one performs the Schrieffer-Wolf transformation on the Hubbard model to eliminate states having doubly occupied sites in the  $U/t \rightarrow \infty$  limit. The result is the familiar  $t$ - $J$  model. In the following we shall adopt the same approach as the one used in the last section. As we shall see, there are two levels of quasiparticle formation. At the first level, like in 1D, we shall find that in the mean-field theory doping in the antiferromagnetic long-range ordered state produces solitons, whose corresponding band structure exhibits states inside the gap. Unlike 1D, the solitons are non-topological. At the second level, due to the residual coupling between the soliton and the spin degrees of freedom, the soliton is further dressed so that the bandwidth associated with its hopping is reduced from  $\sim t$  to  $\sim J$ . In 1D the second level of renormalization is absent.

### A. Mean-field solution for one hole

The Hubbard-Stratonovich decoupling scheme and the subsequent mean-field ansatz are the same as in 1D. In particular, the mean-field Hamiltonian is

$$H_{mf} = -t \sum_{\langle i,j \rangle} \left( c_i^\dagger c_j + h.c. \right) + \sum_j c_j^\dagger \left[ \Delta_c^{(0)}(j) + (-1)^{j_x+j_y} \Delta_s^{(0)}(j) \sigma_z \right] c_j + \frac{1}{U} \sum_j \left\{ \left[ \Delta_s^{(0)}(j) \right]^2 - \left[ \Delta_c^{(0)}(j) \right]^2 \right\}. \quad (40)$$

The only difference is that now  $i, j$  label the square lattice sites. The corresponding saddle point equations are similar to Eq. (27) and (28),

$$\Delta_s^{(0)}(i) = -(-1)^{i_x+i_y} \frac{U}{2} \left[ \langle c_{i\uparrow}^\dagger c_{i\uparrow} \rangle - \langle c_{i\downarrow}^\dagger c_{i\downarrow} \rangle \right]. \quad (41)$$

$$\Delta_c^{(0)}(i) = \frac{U}{2} \left[ \langle c_{i\uparrow}^\dagger c_{i\uparrow} \rangle + \langle c_{i\downarrow}^\dagger c_{i\downarrow} \rangle \right]. \quad (42)$$

We solve the above equations numerically on a  $14 \times 14$  lattice with periodic boundary condition. The number of electrons is such that there is only one hole. We have chosen three different starting points for the self-consistent iteration. In each case, we reduce the Néel order parameter from its value at half-filling symmetrically around a lattice site, lattice link, and the center of a plaquette respectively. For  $U/t$  not too small (say  $U/t \geq 10/3$ ), the first two starting points converge to a non-topological soliton centered on a lattice site. We have also checked that a small perturbation in the starting configuration does not affect the final self-consistent solution. The magnitude of the resulting order parameter has a fourfold rotational symmetry about the center. For  $U/t \geq 10/3$ , the third starting point first converges to a diagonal cigar-shaped non-topological soliton situated at the plaquette center. However, if we slightly break the reflection symmetry about the plaquette center along the ridge of the diagonal cigar-shaped spin profile, the iteration further converges to the same solution as found from the previous two starting points. For  $U/t \geq 10/3$ , the self-consistent mean-field solutions are non-topological solitons. The typical spin and charge density profiles are shown in Fig. 10, and the corresponding mean-field band structure is shown in Fig. 11. We note that two midgap states are present. For one hole, only states in the lower band are occupied. The energies of the soliton with respect to a hole at the top of the valence band of the half-filled band structure are  $\delta E = -0.051t (-0.049\Delta_s^{(0)})$  for  $U/t = 10/3$ ,  $-0.386t (-0.155\Delta_s^{(0)})$  for  $U/t = 6$ ,  $-0.650t (-0.182\Delta_s^{(0)})$  for  $U/t = 8$ ,  $-0.858t (-0.185\Delta_s^{(0)})$  for  $U/t = 10$ , and  $-1.017t (-0.179\Delta_s^{(0)})$  for  $U/t = 12$ . For  $U/t \geq 8$ , the calculations are done in  $10 \times 10$  lattice since the finite size effect is small for large  $U/t$  ratios.

In Fig. 12, we show the changes in the spin density induced by a soliton. We have checked numerically that  $\sum_{i,\sigma} \delta \langle c_{i\sigma}^\dagger c_{i\sigma} \rangle = -1$  and  $|\sum_i \delta \langle S_i^z \rangle| = 1/2$ . Thus, unlike 1D, the soliton carries both charge and spin.

The same mean-field studies for one hole in the 2D Hubbard model has been carried out by Su and Chen,<sup>6</sup> and Choi and Mele.<sup>7</sup> For large  $U/t$  our results are consistent with their findings. For example, we have found that for  $U/t \geq 10/3$ , the saddle point solution is a soliton whose associated spatial variation of the Néel order parameter respects the fourfold rotational symmetry of the underlying lattice. Moreover, our self-consistent band structure agrees with that found in Ref. 6 (for  $U/t = 5$  on  $10 \times 10$  lattice) within numerical uncertainties. However, for smaller  $U/t$  (say  $U/t = 2$ ) we found that unlike previous claims that the solitons are cigar-shaped, after a large number of self-consistent iterations the soliton converges to a linear bag running diagonally across the whole finite lattice. Based on the length scale defined by  $v_F/2\Delta_s^{(0)}$  we expect significant finite size effects for small  $U/t$ . In addition, for small  $U/t$  the detailed structure of the non-interacting band (such as the magnitude of the next nearest neighbor hopping) starts to have a stronger effect on the soliton shape. At present we have not studied enough lattice sizes and different boundary condition to establish that the extended soliton is the genuine solution in the thermodynamic limit. In that context it is interesting to observe that Schulz<sup>44</sup> suggested that at finite hole concentration, the carriers segregate into linear walls separating  $\pi$ -phase-shifted antiferromagnetic domains. We take the appearance of one-hole line-shaped soliton for small  $U/t$  in our study as an indication in favor of the former possibility.

The saddle point solution for large  $U/t$  is robust and simple to understand. Numerically we have found that when  $U/t$  is increased, the size of the soliton is reduced. Since the soliton has the same quantum numbers as a *bare hole* in the  $t$ - $J$  model, we interpret it as a finite  $U$  analog of the latter, which, among other things, also implies that the mean-field solitons obey Fermi statistics. In the following we shall show that the low-energy fluctuations around the saddle point solution is precisely the low-energy dynamics described by the  $t$ - $J$  model:

$$H_{t-J} = -t \sum_{\langle i,j \rangle} [(1 - n_{i,-\sigma})c_{i\sigma}^\dagger c_{j\sigma}(1 - n_{j,-\sigma}) + h.c.] + J \sum_{\langle i,j \rangle} \vec{S}_i \cdot \vec{S}_j. \quad (43)$$

In the context of our above discussions the perfect Néel state is the analog of our half-filled mean-field solution, and  $c_{i\sigma}$  acting on the latter produces our soliton. The remaining dynamics (including the hopping of the soliton and the flipping of the spins) described by  $H_{t-J}$  are captured by fluctuations around the saddle point.

The derivation of the effective action is similar to the 1D case. However, unlike in 1D, the 2D solitons do have preferential positions (i.e. the sites) even for small  $U/t$ . Thus instead of a continuum description, we use a tight-binding language to describe the soliton hopping. The resulting effective action contains a  $O(3)$  non-linear sigma model part describing the antiferromagnetic fluctuation, and a tight-binding spinless fermion part representing the soliton hopping on the lattice. Finally, unlike in 1D, the soliton motion does couple to the  $\sigma$  model fluctuation. This effective action is precisely the coherent-state functional-integral action of the  $t$ - $J$  model in the slave-fermion + Schwinger boson representation. The details are supplied in Appendix B.

## B. Dressing the non-topological solitons

In the above we have argued that the effective Hamiltonian governing the motion of the solitons and the antiferromagnetic fluctuations is the  $t$ - $J$  model. Due to the residual coupling between spin and charge, the soliton motion in 2D is a highly nontrivial problem. A lot of work has been done on this subject in this context. In particular, two of us have recently presented an intuitive picture that explains how the frustration of hopping in an antiferromagnetic background renormalizes the hole bandwidth from  $\sim t$  to  $\sim J$ .<sup>20</sup>

The question of charge motion in the presence of finite doping concentration is a much more subtle issue. This is due to the following facts. *i)* At finite doping it is not clear what is the best saddle-point solution. For example is the anti-phase domain wall solution suggested by Schultz the correct mean-field solution for certain range of  $U/t$ ? *ii)* Even one assumes that the individual bag-like solitons remain the lowest-energy mean-field solution, one still has to face the fact that in 2D, due to the residual coupling between the solitons and the antiferromagnetic fluctuations, the solitons are further dressed into quasiparticles. When the size of the one-hole quasiparticle reaches the inter-hole spacing the meaning of a quasiparticle is no longer clear. Moreover, the presence of finite carrier concentration may feed back to qualitatively change the low-energy dynamics of the antiferromagnetic fluctuations. Thus even though in the case of one hole, one has reasonable confidence that the bag-like soliton is first formed and subsequently is dressed into a quasiparticle, the same conclusion should be subject to critical scrutiny in the case of finite doping concentration.<sup>45</sup>

With these caveats in mind let us imagine that the doping level is relatively low so that we can view the finite doping as a collection of one-hole quasiparticles. Let us imagine that the magnetic long-range order is destroyed. Let us use the antiferromagnetic fluctuations with wavelength shorter than the magnetic correlation length to dress the soliton<sup>20</sup>. What remains is to determine the effective theory governing the motion of these dressed objects that includes their interaction with the remaining long wavelength magnetic fluctuations.

Since the residual long wavelength spin excitations correspond to smooth fluctuations of the spin directions we describe it by a non-linear  $\sigma$  model (see Appendix B for derivation),

$$S_{\text{nlsm}} = \frac{\rho_s}{2} \int_0^\beta d\tau \int d^2r \sum_{\mu=c_s\tau, x, y} \text{Tr} (\partial_\mu g \partial_\mu g^\dagger + \sigma_z g \partial_\mu g^\dagger \sigma_z g \partial_\mu g^\dagger), \quad (44)$$

where  $\rho_s$  is the stiffness and  $c_s$  is the spin wave velocity. In particular, we choose  $\rho_s$  so that the resulting  $\sigma$  model is in the disordered phase. (Here we should point out the fact that how to get a spin liquid described by the disordered  $\sigma$  model from a microscopic spin model on a lattice is still an open issue.) To find the effective action for the quasiparticle propagation, we need to generalize the quasiparticle construction in Ref. 20 to allow a smoothly fluctuating spin background. Since the dressing envisioned in Ref. 20 is a short wavelength and high-energy process, it will not be significantly affected as long as the spin correlation length and correlation time are sufficiently long. The generalized construction of the quasiparticle for the  $t$ - $J$  model is described in Appendix B, where the soliton hopping is treated exactly while the spin-exchange part is treated on average. The quantum spin fluctuation generates hopping of the dressed object as a whole. Let  $i$  and  $j$  be two lattice sites with quasiparticle creation operators  $f_i^\dagger$  and  $f_j^\dagger$ . The hopping matrix element between these two states is due to the spin exchange part of the  $t$ - $J$  Hamiltonian,  $H_J = J \sum_{\langle i,j \rangle} \vec{S}_i \cdot \vec{S}_j$ . With only short range order, the local spin directions at the sites  $i$  and  $j$  are not necessarily parallel to each other. Since the quasiparticle spins are constrained to follow the local spin directions, the two quasiparticle states at the sites  $i$  and  $j$  do not have parallel spin directions. As a result, the hopping amplitude

acquires a Berry phase which is expressed in terms of the SU(2) matrix  $g(i)$ . The details of the derivation are included in Appendix B. Taking into account this additional factor, the quasiparticle hopping is described by,

$$H_{\text{qp}} = \sum_{i \in \mathcal{A}, r = \sqrt{2}, 2} \alpha(r) [g(i)g^+(i+r)]_{11} f_i^\dagger f_{i+r} + \sum_{i \in \mathcal{B}, r = \sqrt{2}, 2} \alpha(r) [g(i)g^+(i+r)]_{22} f_i^\dagger f_{i+r} + \sum_{i \in \mathcal{A}, r = \sqrt{5}, 3} \lambda(r) \left\{ [g(i)g^+(i+r)]_{12} f_i^\dagger f_{i+r} + h.c. \right\}, \quad (45)$$

where the matrix subscript denotes the respective element, and the notation  $r = \sqrt{2}$ , for example, indicates summing over all neighboring sites of  $\sqrt{2}$  units of lattice constant. The first two terms of Eq. (45) represent the hopping among the same sublattice sites, while the last one describes the quasiparticle hopping term between different sublattices. Long range hopping farther than three lattice spacings has been neglected. We expect that the results for the coefficients  $\alpha(r)$  and  $\lambda(r)$  calculated in Ref. 20 remain a good estimate so long as the correlation length (or time) of the antiferromagnetic order remains long. The two parameters,  $\alpha(\sqrt{2})$  and  $\alpha(2)$ , describe a quasiparticle band of a width of order  $2J$ , with the minimum at  $(\pi/2, \pi/2)$  and extended van Hove regions around  $(\pi, 0)$  and  $(0, \pi)$ .<sup>8-13, 21-26</sup> Alternatively, these parameters, as well as  $\lambda(r)$ , can also be taken as phenomenological parameters of the effective theory to be determined from fitting experimental data.

Using the representation (22) of the SU(2) matrix, Eq. (45) can be recast as

$$H_{\text{qp}} = \sum_{i \in \mathcal{A}, 2, 2} \alpha(r) \sum_{\sigma} z_{\sigma}^*(i) z_{\sigma}(i+r) f_i^\dagger f_{i+r} + \sum_{i \in \mathcal{B}, r = \sqrt{2}, 2} \alpha(r) \sum_{\sigma} z_{\sigma}(i) z_{\sigma}^*(i+r) f_i^\dagger f_{i+r} + \sum_{i \in \mathcal{A}, r = \sqrt{5}, 3} \lambda(r) \left\{ [z_1^*(i) z_2^*(j+r) - z_2^*(i) z_1^*(i+r)] f_i^\dagger f_{i+r} + h.c. \right\}. \quad (46)$$

The corresponding part of the action is

$$S_{\text{qp}} = \int_0^\beta d\tau \left( \sum_i \bar{f}_i \partial_\tau f_i + H_{\text{qp}} \right). \quad (47)$$

The complete effective action is

$$S_{\text{eff}} = S_{\text{nls}} + S_{\text{qp}}. \quad (48)$$

### C. Closing remarks

What can be said about the nature of the carriers after being dressed by both short and long ranged magnetic fluctuations? For one hole in an antiferromagnet it is widely believed that the soliton is dressed into a quasiparticle. Here we quote some numerical results. For the  $t$ - $J$  model there exists direct diagonalization results.<sup>8-13</sup> The conclusion of these studies paints a picture in favor of a quasiparticle with internal structure. These results can be understood in the string picture developed in Ref. 20. For the 2D Hubbard model, most numerical results are obtained from Monte-Carlo simulations.<sup>21, 22</sup> Unlike the direct diagonalization, these results are for non-zero temperatures. Moreover, it is often hard to obtain very low temperature results. In any case the state-of-the-art low temperature Monte-Carlo results agree with the  $t$ - $J$  model diagonalization. The outcome is a quasiparticle obeying a dispersion relation best fitted to<sup>12, 21-26</sup>

$$\epsilon_{\vec{k}} = 4\alpha(\sqrt{2}) \cos k_x \cos k_y + 2\alpha(2)(\cos 2k_x + \cos 2k_y). \quad (49)$$

The two parameters  $\alpha(\sqrt{2})$  and  $\alpha(2)$  have also been calculated in the string picture.<sup>20</sup> This result compares very favorably with the Angle-Resolved Photoemission results of the high temperature superconductors near optimum doping.<sup>46-48</sup>

In the presence of a finite concentration of holes, it is far less clear whether the quasiparticle picture is correct. The effective Hamiltonian, given by Eqs. (44) and (45), describes the ultimate dressing of the quasiparticles which have already been partially dressed by short wavelength antiferromagnetic fluctuations. The best chance for the relevance of the Hamiltonian is when the magnetic correlation length (time) is long compared with the inter-hole spacing (inverse intra-quasiparticle excitation gap). This Hamiltonian has been postulated and studied by a number of authors.<sup>27-30</sup> Here we have presented a derivation of it.

## V. CONCLUSION

In this paper we have demonstrated that the two low-energy dynamical degrees of freedom in doped Hubbard model are *a*) soliton charge carriers, and *b*) smooth antiferromagnetic fluctuations. We have arrived at these excitations starting from the SDW mean-field theory. The quantum number of the charge soliton distinguishes one dimension from the rest. In 1D the charge solitons are the anti-phase domain wall of the longitudinal spin order. They carry no  $\langle S^z \rangle$ , consequently they do not suffer from further dressing by the magnetic fluctuations. Thus in 1D the final effective theory is a decoupled charge and spin model. In two dimensions, the solitons are bag-like objects and they do carry  $\langle S^z \rangle$ . Consequently, they are further dressed by the antiferromagnetic fluctuations. The ultimate effective theory consists of two types of charged particles, i.e. with opposite fictitious charge, coupled to fluctuating gauge fields. The final zero temperature state of such model is currently not known.

At last, it is important to point out that in two space dimensions we made an important assumption at finite doping — that individual solitons are still the lowest-energy mean-field solution. If that turns out wrong, and if the charged object has the form of an extended domain wall, then the discussions presented here are irrelevant.

## ACKNOWLEDGMENTS

The authors thank Safi Bahcall for valuable comments on the manuscript.

## APPENDIX A: TAKAYAMA-LIN-LIU-MAKI EQUATION

The one-dimensional Hubbard model written in the form of Eq. (11) does not resemble the Su-Schrieffer-Heeger model<sup>17</sup> describing Polyacetylene in the lattice even if the transverse fluctuations of the spin directions are turned off. One difference is that the longitudinal spin order  $\Delta_s(i)$  does not have dynamics in Eq. (11). In other words, Eq. (11) does not contain time derivative of  $\Delta_s(i)$ . This difference is not so important since the quantum fluctuations will generate dynamics for  $\Delta_s(i)$ . Another difference lies in the way how the longitudinal spin order is coupled to the electrons. Despite these differences, we show in the following that the continuum version of the saddle point equations corresponding to Eq. (26) are essentially the same as the Takayama-Lin-Liu-Maki equation<sup>37</sup> determining the soliton solution in the continuum for Polyacetylene.

In the continuum limit, we substitute into Eq. (26)

$$c_j = e^{ik_F R_j} \psi_L(j) + e^{-ik_F R_j} \psi_R(j), \quad R_j = ja, \quad (\text{A1})$$

where  $\psi_{L,R}(i)$  are slowly varying fields in space,  $\psi_L^\dagger(j) = (\psi_{L\uparrow}^\dagger(j), \psi_{L\downarrow}^\dagger(j))$ ,  $k_F a = \pi/2$  at the half filling, and  $a$  is the lattice constant. The saddle point Hamiltonian, Eq. (26), becomes

$$\begin{aligned} H_{mf} = & -2ta \sum_j \left[ \psi_L^\dagger(j) i \partial_x \psi_L(j) - \psi_R^\dagger(j) i \partial_x \psi_R(j) \right] + \sum_j \Delta_c^{(0)}(j) \left[ \psi_L^\dagger(j) \psi_L(j) + \psi_R^\dagger(j) \psi_R(j) \right] \\ & + \sum_j \Delta_s^{(0)}(j) \left[ \psi_L^\dagger(j) \sigma_z \psi_R(j) + \psi_R^\dagger(j) \sigma_z \psi_L(j) \right] + \frac{1}{U} \sum_j \left\{ \left[ \Delta_s^{(0)}(j) \right]^2 - \left[ \Delta_c^{(0)}(j) \right]^2 \right\}. \end{aligned} \quad (\text{A2})$$

The discrete summation can be converted into integration according to

$$a \sum_j \rightarrow \int dx; \quad \frac{1}{\sqrt{a}} \psi_{L,R}(j) \rightarrow \psi_{L,R}(x); \quad \Delta_{c,s}^{(0)}(j) \rightarrow \Delta_{c,s}^{(0)}(x). \quad (\text{A3})$$

The two spin components are decoupled in the above mean field Hamiltonian. The mean field Hamiltonian can be rewritten as

$$\begin{aligned} H_{mf} = & \sum_{\alpha=\pm} \int dx \left[ \psi_{L\alpha}^\dagger, \psi_{R\alpha}^\dagger \right] \left[ -iv_F \sigma_z \partial_x + \Delta_c^{(0)}(x) + \alpha \Delta_s^{(0)}(x) \sigma_x \right] \begin{bmatrix} \psi_{L\alpha}(x) \\ \psi_{R\alpha}(x) \end{bmatrix} \\ & + \frac{1}{Ua} \int dx \left\{ \left[ \Delta_s^{(0)}(x) \right]^2 - \left[ \Delta_c^{(0)}(x) \right]^2 \right\}, \end{aligned} \quad (\text{A4})$$

where  $v_F = 2ta$ ,  $\sigma_z$  and  $\sigma_x$  are Pauli matrices. The spin index  $\alpha = \pm$  corresponds to spin up and down respectively. This continuum version of the saddle point Hamiltonian has the similar form as the continuum Hamiltonian for Polyacetylene.<sup>37</sup> Expanding the operators  $\psi_{L,R}(x)$  in terms of their eigenfunctions

$$\psi_{L\alpha}(x) = \sum_{\kappa} u_{\kappa,\alpha}(x) \psi_{L\alpha}(\kappa), \quad (\text{A5})$$

$$\psi_{R\alpha}(x) = \sum_{\kappa} v_{\kappa,\alpha}(x) \psi_{R\alpha}(\kappa), \quad (\text{A6})$$

the corresponding saddle point equations are very similar to Takayama-Lin-Liu-Maki equation,<sup>37</sup>

$$-iv_F \partial_x u_{\kappa,\alpha}(x) + \Delta_c^{(0)}(x) u_{\kappa,\alpha}(x) + \alpha \Delta_s^{(0)}(x) v_{\kappa,\alpha}(x) = \epsilon_{\kappa,\alpha} u_{\kappa,\alpha}(x), \quad (\text{A7})$$

$$iv_F \partial_x v_{\kappa,\alpha}(x) + \Delta_c^{(0)}(x) v_{\kappa,\alpha}(x) + \alpha \Delta_s^{(0)}(x) u_{\kappa,\alpha}(x) = \epsilon_{\kappa,\alpha} v_{\kappa,\alpha}(x), \quad (\text{A8})$$

$$\Delta_s^{(0)}(x) = -\frac{Ua}{2} \sum_{\alpha=\pm} \sum_{\kappa \in \text{occup}} \alpha [u_{\kappa,\alpha}^*(x) v_{\kappa,\alpha}(x) + v_{\kappa,\alpha}^*(x) u_{\kappa,\alpha}(x)], \quad (\text{A9})$$

$$\Delta_c^{(0)}(x) = \frac{Ua}{2} \sum_{\alpha=\pm} \sum_{\kappa \in \text{occup}} [|u_{\kappa,\alpha}(x)|^2 + |v_{\kappa,\alpha}(x)|^2]. \quad (\text{A10})$$

The only difference is the appearance of an additional self-consistent equation for  $\Delta_c^{(0)}(x)$ . This analogy underlies the common physics of the holon in 1D Hubbard model and soliton in Polyacetylene. From this analogy, we identify the counterpart of the dimensionless electron-phonon coupling constant  $\lambda_{e-ph}$  of the Polyacetylene<sup>16</sup> to be

$$\frac{1}{2\pi v_F \lambda_{e-ph}} = \frac{1}{Ua}, \quad \Rightarrow \quad \lambda_{e-ph} = \frac{U}{4\pi t}. \quad (\text{A11})$$

In the absence of the self-consistent equation for  $\Delta_c^{(0)}(x)$ , the saddle point equations have been solved in closed form giving rise to  $\Delta_s^{(0)}(x) = \Delta_s^{(0)} \tanh(x/\xi)$ . The electron density calculated using the eigenfunctions in the presence of the kink has a shallow dip at the kink position which has the form  $1 - 1/[2\xi \cosh^2(x/\xi)]$ . This shallow dip causes additional scattering effects when there is an additional equation for  $\Delta_c^{(0)}(x)$ . Although the true solution in this case will be different from that in Polyacetylene, we expect that the difference is only quantitative. In particular, the change should not be significant when  $\xi \gg 1$ , i.e. for small  $U/t$ .

The presence of the Hartree term distinguishes the continuum equations in this case from those in Polyacetylene. However, the localized states are still degenerate in the spin index. To see this, let us define

$$f_{\alpha}^{(\pm)}(x) = u_{\alpha}(x) \pm v_{\alpha}(x). \quad (\text{A12})$$

The coupled equations for  $u_{\alpha}(x)$  and  $v_{\alpha}(x)$  (the index  $\kappa$  is omitted) become

$$-i \left[ v_F \partial_x \pm \alpha \Delta_s^{(0)}(x) \right] f_{\alpha}^{(\pm)}(x) = \left[ \epsilon_{\alpha} - \Delta_c^{(0)}(x) \right] f_{\alpha}^{(\mp)}(x). \quad (\text{A13})$$

We see that the equations are invariant under  $f_{\uparrow}^{(+)} \rightarrow f_{\downarrow}^{(-)}$  and  $f_{\uparrow}^{(-)} \rightarrow f_{\downarrow}^{(+)}$ .

## APPENDIX B: CALCULATION OF THE FLUCTUATIONS AROUND THE SADDLE POINT

The general formalism of calculating Gaussian fluctuations is as follows. Substituting into Lagrangian (11) the expansion

$$\Delta_s(j) = \Delta_s^{(0)}(j) + \delta\Delta_s(j), \quad (\text{B1})$$

$$\Delta_c(j) = -i\Delta_c^{(0)}(j) + \delta\Delta_c(j), \quad (\text{B2})$$

we separate the full Lagrangian, of the form of Eq. (11) into a mean-field part and a fluctuation part.

$$\mathcal{L} = \mathcal{L}_{mf} + \delta\mathcal{L}, \quad (\text{B3})$$

$$\mathcal{L}_{mf} = \sum_{i,j} \sum_{\mu,\nu} \bar{c}_{i,\mu} \left( \partial_{\tau} + h_{\{i,\mu\},\{j,\nu\}}^{(0)} \right) c_{j,\nu} + \mathcal{L}_0(\delta\Delta_c, \delta\Delta_s), \quad (\text{B4})$$

$$\delta\mathcal{L} = \sum_{i,j} \sum_{\mu,\nu} \bar{c}_{i,\mu} \left[ h^{(1)}(\delta\Delta_c, \delta\Delta_s, g) \right]_{\{i,\mu\},\{j,\nu\}} c_{j,\nu}. \quad (\text{B5})$$

The time-independent matrix  $h^{(0)}$  can be specified once the saddle point solution is obtained. The matrix  $h^{(1)}$  depends on the fluctuating fields  $\delta\Delta_c(j)$ ,  $\delta\Delta_s(j)$  and  $g$ . The quadratic part,

$$\mathcal{L}_0(\delta\Delta_c, \delta\Delta_s) = (1/U) \sum_i \left\{ [\delta\Delta_s(i)]^2 + [\delta\Delta_c(i)]^2 \right\}, \quad (\text{B6})$$

is unaffected by the procedure of integrating out fermions to obtain the effective action defined through

$$e^{-S_{\text{eff}}(\delta\Delta_c, \delta\Delta_s, g)} = \int \mathcal{D}[c, \bar{c}] e^{-\int_0^\beta d\tau \mathcal{L}}. \quad (\text{B7})$$

The integration is carried out mainly by expansion. The first step of the calculation is to diagonalize  $\mathcal{L}_{mf}$ . This is achieved by a linear transformation,

$$\bar{c}_{j,\sigma} = \sum_{\kappa} \alpha_{\kappa,j}^{(\sigma)} \bar{\psi}_{\kappa,\sigma}. \quad (\text{B8})$$

To have a Jacobian equal to 1 or to preserve the proper commutation relation  $\{\psi_{\kappa_1,\sigma}^\dagger, \psi_{\kappa_2,\sigma}\} = \delta_{\kappa_1,\kappa_2}$  in the operator language, the transformation coefficients  $\alpha_{\kappa,j}^{(\sigma)}$  must satisfy

$$\sum_{\kappa} \alpha_{\kappa,i}^{(\sigma)*} \alpha_{\kappa,j}^{(\sigma)} = \delta_{i,j}. \quad (\text{B9})$$

In terms of the new Grassmann variables  $\psi_{\kappa,\sigma}$  and  $\bar{\psi}_{\kappa,\sigma}$ , the mean-field Lagrangian is diagonalized,

$$\mathcal{L}_{mf} = \sum_{\kappa,\sigma} \bar{\psi}_{\kappa,\sigma} (\partial_\tau + \epsilon_{\kappa,\sigma}) \psi_{\kappa,\sigma} + \mathcal{L}_0(\delta\Delta_c, \delta\Delta_s), \quad (\text{B10})$$

where  $\epsilon_{\kappa,\sigma}$  is the eigenvalue of the matrix  $h^{(0)}$ . Then, we can represent the interaction part of the Lagrangian in terms of the new variables  $\psi_{\kappa,\sigma}$  and  $\bar{\psi}_{\kappa,\sigma}$ ,

$$\delta\mathcal{L} = \sum_{\kappa_1,\kappa_2} \sum_{\mu,\nu} \bar{\psi}_{\kappa_1,\mu}(\tau) h_{\kappa_1,\kappa_2}^{(\mu,\nu)}(\tau) \psi_{\kappa_2,\nu}(\tau), \quad (\text{B11})$$

where

$$h_{\kappa_1,\kappa_2}^{(\mu,\nu)}(\tau) = \sum_{i,j} \alpha_{\kappa_1,i}^{(\mu)*} \left[ h^{(1)}(\delta\Delta_c, \delta\Delta_s, g) \right]_{\{i,\mu\},\{j,\nu\}} \alpha_{\kappa_2,j}^{(\nu)}. \quad (\text{B12})$$

In the final step, we expand the interaction  $\delta\mathcal{L}$  in the partition function. To the first order,

$$\langle \delta\mathcal{L} \rangle = \sum_{\kappa_1,\kappa_2} \sum_{\mu,\nu} h_{\kappa_1,\kappa_2}^{(\mu,\nu)} \langle \bar{\psi}_{\kappa_1,\mu}(\tau) \psi_{\kappa_2,\nu}(\tau) \rangle. \quad (\text{B13})$$

In the second order of the expansion in  $\delta\mathcal{L}$ , the generated effective action is

$$S_{\text{eff}}^{(2)} = \frac{1}{2} \sum_{\nu_n} \sum_{\kappa_1,\kappa_2} \sum_{\mu,\nu} \Pi_{\mu,\nu}(\kappa_1, \kappa_2, \nu_n) h_{\kappa_1,\kappa_2}^{(\mu,\nu)}(\nu_n) h_{\kappa_2,\kappa_1}^{(\nu,\mu)}(-\nu_n), \quad (\text{B14})$$

where  $\nu_n = 2\pi n/\nu$  is the Bosonic Matsubara frequency, and  $h_{\kappa_1,\kappa_2}^{(\mu,\nu)}(\nu_n)$  is the Fourier transform of  $h_{\kappa_1,\kappa_2}^{(\mu,\nu)}(\tau)$ . The function  $\Pi_{\mu,\nu}(\kappa_1, \kappa_2, \nu_n)$  has the usual Lindhard form

$$\Pi_{\mu,\nu}(\kappa_1, \kappa_2, \nu_n) = \frac{f(\epsilon_{\kappa_1,\mu}) - f(\epsilon_{\kappa_2,\nu})}{i\nu_n + \epsilon_{\kappa_1,\mu} - \epsilon_{\kappa_2,\nu}}, \quad (\text{B15})$$

where  $f(\epsilon) = 1/(1 + e^{\beta\epsilon})$  is the Fermi-Dirac distribution function. Since the particle-hole excitation in the spectrum of the mean-field state has an energy gap, we can safely approximate  $\Pi_{\mu,\nu}(\kappa_1, \kappa_2, \nu_n) \simeq \Pi_{\mu,\nu}(\kappa_1, \kappa_2, 0)$ . In the rest of this section, we shall apply this procedure of obtaining effective action to both 1D and 2D Hubbard model.

## 1. One-dimensional case

Substituting Eqs. (36) and (B2) into Eq. (11), the full 1D Lagrangian is written as

$$\begin{aligned} \mathcal{L} = & \sum_j \bar{c}_j \left[ \partial_\tau - \tilde{\mu} + i \delta\Delta_c(j) + g(j) \partial_\tau g^+(j) + \Delta_s^{(0)} \cos(2k_F R_j + \Phi_j) \sigma_z \right] c_j \\ & - t \sum_{\langle i,j \rangle} [\bar{c}_i g(i) g^+(j) c_j + h.c.] + \frac{[\Delta_s^{(0)}]^2}{U} \sum_j \cos^2(2k_F R_j + \Phi_j) + \frac{1}{U} \sum_j [\delta\Delta_c(j)]^2. \end{aligned} \quad (\text{B16})$$

In one dimension, we can simplify the Lagrangian by taking the continuum limit. The fermion fields can be linearized around the Fermi surface, which consists of two points in one dimension. This is done by Eq. (A1) but with  $k_F = \pi(1 - n_h)/2$  in the general case. Since  $\Phi(i)$  and  $g(i)$  are slowly varying functions, we can expand

$$g(i)g^+(j) - 1 = ag(i)\partial_x g^+(i) + \frac{a^2}{2}g(i)\partial_x^2 g^+(i) + \dots,$$

where  $a$  is the lattice constant. Using this expansion, we find

$$\begin{aligned} -t \sum_{\langle i,j \rangle} [\bar{c}_i g(i) g^+(j) c_j + h.c.] = & -v_F \sum_j \left\{ \psi_L^\dagger(j) [i\partial_x + g(j)i\partial_x g^+(j)] \psi_L(j) - (L \rightarrow R) \right\} \\ & - ta^2 \cos(k_F a) \sum_j \left[ \psi_L^\dagger(j) g(j) \partial_x^2 (g^+(j) \psi_L(j)) + (L \rightarrow R) \right], \end{aligned} \quad (\text{B17})$$

where we have denoted

$$v_F = 2ta \sin(k_F a). \quad (\text{B18})$$

This generalizes the definition of  $v_F$  to the arbitrary electron filling factor. Similarly, we have

$$\Delta_s^{(0)} \sum_j \bar{c}_j \cos(2k_F R_j + \Phi_j) \sigma_z c_j = \begin{cases} \Delta_s^{(0)} \cos \Phi_j [\psi_L^\dagger(j) \sigma_z \psi_R(j) + h.c.], & \text{for } k_F a = \pi/2, \\ \frac{1}{2} \Delta_s^{(0)} [e^{i\Phi_j} \psi_L^\dagger(j) \sigma_z \psi_R(j) + h.c.], & \text{for } k_F a \neq \pi/2. \end{cases} \quad (\text{B19})$$

We also note that

$$2 \sum_i \cos^2(2k_F R_i + \Phi_i) = \mathcal{N} + \sum_i \cos(4k_F R_i + 2\Phi_i) \simeq \begin{cases} \mathcal{N}, & \text{for } k_F a \neq \pi/2, \\ \mathcal{N} + \sum_i \cos(2\Phi_i), & \text{for } k_F a = \pi/2. \end{cases} \quad (\text{B20})$$

The other terms in Eq. (B16) are simplified in the same way. In the case of finite doping,  $k_F a \neq \pi/2$ , we can redefine the fermion fields to absorb the phase  $e^{i\Phi_j}$  accompanying  $\Delta_s^{(0)}$  in Eq. (B19),

$$\tilde{\psi}_L(j) = \psi_L(j) e^{-i\Phi_j/2}, \quad \tilde{\psi}_R(j) = \psi_R(j) e^{i\Phi_j/2}. \quad (\text{B21})$$

Substituting Eqs. (B17) through (B21) into Eq. (B16), we obtain for the case of finite doping,

$$\begin{aligned} \mathcal{L}_{mf} = & \int dx \left[ \tilde{\psi}_L^\dagger(x), \tilde{\psi}_R^\dagger(x) \right] \begin{bmatrix} \partial_\tau - iv_F \partial_x & \frac{1}{2} \Delta_s^{(0)} \sigma_z \\ \frac{1}{2} \Delta_s^{(0)} \sigma_z & \partial_\tau + iv_F \partial_x \end{bmatrix} \begin{bmatrix} \tilde{\psi}_L(x) \\ \tilde{\psi}_R(x) \end{bmatrix} \\ & + \mathcal{N} \frac{[\Delta_s^{(0)}]^2}{2U} + \frac{1}{Ua} \int dx [\delta\Delta_c(x)]^2, \end{aligned} \quad (\text{B22})$$

$$\delta\mathcal{L} = \int dx \left[ \tilde{\psi}_L^\dagger(x) A_L(x) \tilde{\psi}_L(x) + \tilde{\psi}_R^\dagger(x) A_R(x) \tilde{\psi}_R(x) \right], \quad (\text{B23})$$

where we have converted the discrete summation into integration according to Eq. (A3) and

$$g(i) \rightarrow g(x), \quad \delta\Delta_c(i) \rightarrow \delta\Delta_c(x). \quad (\text{B24})$$



We have also introduced the notations,

$$A_{L,R}(x) = g(x)(\partial_\tau \mp iv_F \partial_x)g^+(x) + \frac{i}{2}(\pm \partial_\tau - iv_F \partial_x)\Phi(x) + i \delta\Delta_c(x). \quad (\text{B25})$$

It is now straightforward to calculate the Gaussian fluctuations according to the general prescription, Eqs. (B4) and (B5). We note that the site index in Eqs. (B4) and (B5) corresponds to the chirality index and the space coordinate in Eq. (B22). The lattice summation corresponds to

$$\sum_i \rightarrow \sum_{\text{chirality}=L,R} \int dx.$$

After Fourier transformation to the momentum  $k$  space, Eq. (B22) is easily diagonalized by a Bogoliubov transformation. For  $\delta\mathcal{L}$  given by Eq. (B23),  $\langle \delta\mathcal{L} \rangle = 0$ . In the second order contribution from  $\delta\mathcal{L}$  expansion, the transverse spin fluctuation part is decoupled from the rest and is given by the non-linear sigma model, Eq. (24). The spin stiffness in Eq. (24) is given by

$$\rho_s = \frac{2v_F^2}{\beta} \sum_{\omega_n} \int \frac{dk}{2\pi} \left| \langle \psi_L^\dagger(k, \omega_n) \psi_R(k, \omega_n) \rangle \right|^2 = \frac{2v_F^2}{\beta} \sum_{\omega_n} \int \frac{dk}{2\pi} \left[ \frac{\Delta_s^{(0)}/2}{\omega_n^2 + (v_F k)^2 + [\Delta_s^{(0)}/2]^2} \right]^2 = \frac{v_F}{2\pi}. \quad (\text{B26})$$

Note that the Gaussian fluctuations only give rise to the second term of Eq. (24). The first term is due to the topological effect in Eqs. (B22) and (B23) which is not captured by the expansion in  $\delta\mathcal{L}$ . When tracing out the fermions, the resulting effective action contains an imaginary term known as the Berry phase. In the language of Eqs. (B22) and (B23), the Berry phase appears in the form of chiral anomaly. Mathematically, the chiral anomaly exists because there is no regularization which preserves both gauge and chiral invariance. Physically, this Berry phase term is the electric field experienced by the phase of the holons  $\Phi(x)$ . This Berry phase has been calculated exactly by Nagaosa and Oshikawa<sup>36</sup> which is given by Eq. (23) with  $\theta = \pi$ , independent of doping. We shall not repeat the calculation here.

The rest of the effective action including up to the second order contributions is

$$S_{\text{eff}}(\Phi, \delta\Delta_c) = \int_0^\beta d\tau \int dx \left\{ \frac{\rho_c^{(0)}}{2} \left[ \frac{1}{v_F^2} (\partial_\tau \Phi)^2 + \left( \partial_x \Phi + \frac{2i}{v_F} \delta\Delta_c(x) \right)^2 \right] + \frac{1}{Ua} [\delta\Delta_c(x)]^2 \right\}, \quad (\text{B27})$$

where  $\rho_c^{(0)} = \rho_s = v_F/2\pi$ . The  $\delta\Delta_c(x)$  fluctuation is gapful and therefore can be integrated out. The remaining low energy mode described by  $\Phi(x)$  has an effective action

$$S_{\text{eff}}(\Phi) = \frac{\rho_c}{2} \int_0^\beta d\tau \int dx \left[ \frac{1}{v_c^2} (\partial_\tau \Phi)^2 + (\partial_x \Phi)^2 \right], \quad (\text{B28})$$

where

$$\rho_c = \rho_c^{(0)} \left( 1 + \frac{Ua}{Ua + \pi v_F} \right) = \frac{v_F}{2\pi} \left( 1 + \frac{Ua}{Ua + \pi v_F} \right), \quad (\text{B29})$$

$$v_c = v_F \sqrt{1 + \frac{Ua}{Ua + \pi v_F}}. \quad (\text{B30})$$

We observe that these coefficients, as well as  $\rho_s$ , are independent of the expectation value  $\Delta_s^{(0)}$ . The increase of the charge stiffness by renormalization indicates that the interaction between the holons is repulsive. The same is true in the doped Polyacetylene.<sup>16</sup>

At half-filling, both Eqs. (B19) and (B20) give different results than at finite doping. We see that a pinning potential proportional to  $\cos 2\Phi$  has appeared, leading to an excitation gap for the bosonic field  $\Phi(x)$ .<sup>18</sup> Thus, only spin excitations are gapless at half-filling. We recover the non-linear sigma model as the effective theory of the 1D Hubbard model at half-filling.

Let us return to the general case of finite doping in one dimension. We have to further show that the various correlation functions can be correctly reproduced using our effective action. Since the effective action we have derived has a form equivalent to the non-Abelian bosonized action, we only need to show that the physical fields entering our effective action have the same meaning as in the non-Abelian bosonization. For this purpose, we can couple external

fields to the spin and charge densities in the original 1D Hubbard model. The rest is to show that the generated external field coupling terms in our effective action have the same forms as those in the non-Abelian bosonization action.

Physically, we have shown in Eq. (38) that  $\partial_x \Phi$  has the meaning of holon density. Since the location of the holon coincides with the hole,  $\partial_x \Phi$  has the meaning of charge density. The size of the holon is irrelevant to the long wavelength physics. Formally, we can also prove that  $\partial_x \Phi$  has the meaning of charge density. We introduce an external potential  $h_c(x, \tau)$  and couple it to the electron density in the original Hubbard model,  $\sum_{i,\sigma} h_c(i, \tau) c_{i\sigma}^\dagger c_{i\sigma}$ . After linearization using Eq. (A1) and phase transformation in Eq. (B21), it becomes

$$\int dx h_c(x, \tau) \left[ \tilde{\psi}_L^\dagger(x) \tilde{\psi}_L(x) + \tilde{\psi}_R^\dagger(x) \tilde{\psi}_R(x) \right] + \int dx h_c(x, \tau) \left[ \tilde{\psi}_R^\dagger(x) \tilde{\psi}_L(x) e^{2ik_F x + i\Phi(x)} + h.c. \right]. \quad (\text{B31})$$

Including the expression (B31) in Eq. (B23), the first term of (B31) adds the potential  $h_c(x, \tau)$  to  $\frac{i}{2}(\pm\partial_\tau - iv_F\partial_x)\Phi(x)$  in  $A_{L,R}(x)$ . When we integrate out the fermionic fields in Eq. (B22), the mixing terms of type  $ih_c(x, \tau)(\pm\partial_\tau - iv_F\partial_x)\Phi(x)$  are generated in the second order. This gives rise to an additional term  $2v_F h_c(x, \tau)\partial_x \Phi(x)$ . Combined with the proper prefactor, the final term in the effective action is indeed  $h_c(x, \tau)\partial_x \Phi(x)/\pi$ . For the second term of (B31), the bilinear fermion operators can be replaced by the saddle point average. This leads to  $2\langle \tilde{\psi}_R^\dagger(x) \tilde{\psi}_L(x) \rangle \int dx h_c(x, \tau) \cos[2k_F x + \Phi(x)]$ . This term will give rise to the oscillating part of the density correlation function.

To show that the vector field  $\vec{n}$  in the effective action represents the spin direction, we couple a magnetic field  $\vec{h}(x, \tau)$  to the spin operator in the original Hubbard model in the form of  $\sum_i \vec{h}(i, \tau) \cdot c_{i\alpha}^\dagger \vec{\sigma}_{\alpha\beta} c_{i\beta}/2$ . Introducing this coupling term into Eq. (7), the last term of Eq. (7) is changed to  $\sum_{i,\alpha\beta} c_{i\alpha}^\dagger [Q_{\alpha\beta}(i) + h_{\alpha\beta}] c_{i\beta} + h.c.$ , where  $h_{\alpha\beta} = (1/4)\vec{h} \cdot \vec{\sigma}_{\alpha\beta}$  and  $Q_{\alpha\beta}(i) = (-1)^i \Delta_s(i) [g^+(i) \sigma_z g(i)]_{\alpha\beta}$ . We can restore the original form for the last term of Eq. (7) by a shift of the integration variable:  $Q_{\alpha\beta} \rightarrow Q_{\alpha\beta}(i) + h_{\alpha\beta}$ . The modification is now transferred to the second term in Eq. (7) which now becomes  $(1/U) \sum_i \text{Tr}|Q+h|^2$ . The mixing term in the expansion of the square of  $Q+h$  is the only relevant magnetic field coupling term which has the form  $(1/U) \sum_i \text{Tr}[\vec{Q}(i)h(i) + h.c.] = (1/U) \sum_i (-1)^i \Delta_s(i) \vec{n}_i \cdot \vec{h}_i$  if we use the fact that  $g^+(i) \sigma_z g(i) = \vec{n}_i \cdot \vec{\sigma}$ . Upon substituting  $(-1)^i \Delta_s(i) = \Delta_s^{(0)} \cos(2k_F R_i + \Phi_i)$  into the above relation, we obtain  $(\Delta_s^{(0)}/U) \sum_i \cos(2k_F R_i + \Phi_i) \vec{n}_i \cdot \vec{h}_i$ . The expressions for the charge and spin density operators and their scaling dimensions should be compared with the non-Abelian bosonization results.<sup>49</sup>

## 2. Two-dimensional case

In two dimensions, the mean-field Lagrangian, the transformation coefficients  $\alpha_{\kappa,j}^{(\sigma)}$  and the eigenenergies  $\epsilon_{\kappa,\sigma}$  are only obtained numerically. In practical calculations, they are all chosen to be real numbers. The saddle point Hamiltonian is given by Eq. (40). The corresponding matrix elements are

$$h_{\{i,\mu\},\{j,\nu\}}^{(0)} = -t \delta_{\mu,\nu} \sum_{r=\pm x, \pm y} \delta_{i-j,r} + \delta_{\mu,\nu} \delta_{i,j} \left[ \Delta_c^{(0)}(i) + \text{sgn}\mu (-1)^{i_x+i_y} \Delta_s^{(0)}(i) \right], \quad (\text{B32})$$

where  $i, j$  label the lattice sites, and  $\mu, \nu$  are the spin indices. The typical  $\Delta_s^{(0)}(i)$  and  $\Delta_c^{(0)}(i)$  for the  $14 \times 14$  lattice are shown in Fig. 10 which is the solution of Eqs. (41) and (42). The transformation coefficients  $\alpha_{\kappa,j}^{(\sigma)}$  are just the eigenvectors obtained by numerically diagonalizing  $h_{\{i,\mu\},\{j,\nu\}}^{(0)}$ . The matrix element in the interaction part of the Lagrangian, Eq. (B5), is identified to be

$$\begin{aligned} \left[ h^{(1)}(\delta\Delta_c(j), \delta\Delta_s(j), g) \right]_{\{l,\mu\},\{j,\nu\}} &= \delta_{l,j} [g(j) \partial_\tau g^+(j)]_{\mu,\nu} - t \sum_{r=\pm x, \pm y} \delta_{l-j,r} [g(l) g^+(j) - 1]_{\mu,\nu} \\ &+ \delta_{l,j} \delta_{\mu,\nu} [i \delta\Delta_c(j) + \text{sgn}\mu (-1)^{j_x+j_y} \delta\Delta_s(j)], \end{aligned} \quad (\text{B33})$$

where  $\delta\Delta_c(j)$ ,  $\delta\Delta_s(j)$  and the SU(2) matrix  $g(j)$  are the fluctuating fields.

The first order term in the expansion of the effective action, Eq. (B13), does not contribute anything interesting since we know that the Berry phase term is canceled out in 2D.<sup>43</sup> In the second order, Eq. (B14), we obtain an action in the variables  $\delta\Delta_c(j)$ ,  $\delta\Delta_s(j)$  and  $g(j)$ . Unlike in the 1D calculation, the coefficients in the effective action have spatial variation since we are perturbing around a saddle point solution which is not uniform in space. The translational invariance will be restored when the soliton motion is included. Thus, we can simply perform the spatial average of the coefficients in  $S_{\text{eff}}^{(2)}$ . Because the soliton has a finite spatial size, although small for  $U/t \gg 1$ , the

effective action  $S_{\text{eff}}^{(2)}$  contains nonlocal terms, such as  $\sum_{i,i'} f(i-i') \text{Tr} [g(i) \partial_\tau g^+(i) g(i') \partial_\tau g^+(i')]$ , where the function  $f(r)$  decreases exponentially with the distance  $r$ . In the momentum space, this nonlocality corresponds to a momentum dependence of the coupling constant which is the spatial Fourier transform of  $f(i-i')$ . If only the long wavelength behavior is concerned, this nonlocality can be neglected by approximating  $\sum_{i,i'} f(i-i') \text{Tr} [g(i) \partial_\tau g^+(i) g(i') \partial_\tau g^+(i')] \simeq \sum_i [\sum_{i'} f(i-i')] \text{Tr} [g(i) \partial_\tau g^+(i) g(i) \partial_\tau g^+(i)]$ . This is equivalent to neglecting the momentum dependence of the coupling constant and taking its value at the momentum  $\vec{k} = 0$ . After the two steps described above, i.e. averaging out the spatial nonuniformity and neglecting the nonlocality of the coefficients in  $S_{\text{eff}}^{(2)}$ , the  $g(j)$  fluctuations are decoupled from  $\delta\Delta_c(j)$  and  $\delta\Delta_s(j)$ . Both  $\delta\Delta_c(j)$  and  $\delta\Delta_s(j)$  fluctuations are gapful. So they can be neglected. The  $g(j)$  fluctuations are described by the non-linear sigma model, Eq. (44), with the stiffness constant given by

$$\rho_s = \frac{t^2}{2\mathcal{N}} \sum_{\kappa,\kappa'} \frac{\theta(\epsilon_{\kappa,\uparrow}) - \theta(\epsilon_{\kappa',\downarrow})}{\epsilon_{\kappa,\uparrow} - \epsilon_{\kappa',\downarrow}} \left[ \sum_i \alpha_{\kappa,i}^{(\uparrow)} \left( \alpha_{\kappa',i+x}^{(\downarrow)} + \alpha_{\kappa',i-x}^{(\downarrow)} \right) \right] \left[ \sum_i \alpha_{\kappa',i}^{(\downarrow)} \left( \alpha_{\kappa,i+x}^{(\uparrow)} + \alpha_{\kappa,i-x}^{(\uparrow)} \right) \right], \quad (\text{B34})$$

where  $\mathcal{N}$  is the number of lattice sites and  $\theta(\epsilon)$  is the step function. The spin wave velocity  $c_s$  is given by

$$\frac{1}{c_s^2} = \frac{1}{2\mathcal{N}\rho_s} \sum_{\kappa,\kappa'} \frac{\theta(\epsilon_{\kappa,\uparrow}) - \theta(\epsilon_{\kappa',\downarrow})}{\epsilon_{\kappa,\uparrow} - \epsilon_{\kappa',\downarrow}} \left( \sum_i \alpha_{\kappa,i}^{(\uparrow)} \alpha_{\kappa',i}^{(\downarrow)} \right)^2. \quad (\text{B35})$$

These expressions can be evaluated using the numerical soliton solution in  $14 \times 14$  lattice for the one-hole problem. The difference of the stiffness from that at half-filling can be viewed as the renormalization due to the hole. In the presence of a finite density of holes, the naive generalization is to multiply the one-hole renormalization by the hole density. However, caution must be exercised if one attempts to apply Eqs. (B34) and Eqs. (B35) to large  $U/t$  ratios. This is because these two expressions involve not only the ground state but also all electron-hole pair excited states. It is reasonable to expect that the mean field solution is a good approximation to the ground state since the self-consistency has been achieved. But the excited states constructed by creating electron-hole pairs in the mean-field spectrum may not be a good approximation of the true charge-excited states of the full Hubbard model.

So far we have calculated the Gaussian fluctuations around the saddle point solution, i.e. the soliton. Therefore, only small fluctuations have been taken into account. Since there are many degenerate saddle point solutions, corresponding to the different locations of the solitons, we must sum up the fluctuation contributions around all saddle point solutions. Furthermore, we must also include the tunneling processes between the different saddle point solutions. In terms of the eigenoperators of the saddle point Hamiltonian corresponding to (B10) whose  $\Delta_s^{(0)}(i)$  profile has a dip located at the site  $i_0$ , the soliton creation operator  $f_{i_0}^\dagger$  is defined through

$$|\text{Bag}(i_0)\rangle = \prod_{\text{Lower bands}} \psi_{\kappa,\sigma}^\dagger |\text{Vacuum}\rangle \stackrel{\text{define}}{=} f_{i_0}^\dagger |\text{SDW}\rangle, \quad (\text{B36})$$

where  $|\text{SDW}\rangle$  is the state without hole. The soliton operator has finite overlap with the bare hole operator in Eq. (B4),

$$c_{i_0,\sigma_0} = \sqrt{Z_{\text{bag}}} f_{i_0}^\dagger + \dots \quad (\text{B37})$$

For a given site,  $\sigma_0$  can only take one value depending on the direction of the magnetization on the site  $i_0$ . Note that the  $\text{SU}(2)$  rotational symmetry is restored by the fluctuating  $g(i)$ . Numerically, it is straightforward to verify, in the  $14 \times 14$  lattice, that  $\sum_{i,\sigma} \delta \langle c_{i\sigma}^\dagger c_{i\sigma} \rangle = -1$  and  $|\sum_i \delta \langle S_i^z \rangle| = 1/2$ . Since all the spatial variations take place locally around the center of the soliton, we have to assign these quantum numbers to the soliton. Similarly, we can take another pair of  $\Delta_s^{(0)}(i)$  and  $\Delta_c^{(0)}(i)$  profiles with exactly the same spatial variation except that the dip is centered on a nearest neighbor site of  $i_0$ . Thus, we construct another soliton in complete analogy with Eq. (B36) and define the soliton creation operator  $f_{j_0}^\dagger$  on the nearest neighbor site of  $i_0$ . If we repeat the calculations determining the quantum numbers of the soliton, we find  $\sum_{i,\sigma} \delta \langle c_{i\sigma}^\dagger c_{i\sigma} \rangle = -1$ , same as before, but  $\sum_i \delta \langle S_i^z \rangle$  has changed sign. So the two solitons constructed above have opposite  $S^z$  quantum numbers. The interaction part of the Hamiltonian corresponding to Eq. (B5) has a nonzero matrix element between these two solitons:

$$\langle \text{Bag}(j_0) | \delta \mathcal{L} | \text{Bag}(i_0) \rangle = -\tilde{t} [g(i_0)g^+(j_0)]_{12}, \quad (\text{B38})$$

where  $\tilde{t} = t \times |\text{overlap integral}|$ . This corresponds to a hopping term of the soliton in the effective action (B7),

$$-\tilde{t} f_{i_0} f_{j_0}^\dagger [g(i_0)g^+(j_0)]_{12}. \quad (\text{B39})$$

Using the representation of the SU(2) matrix  $g(i)$ , i.e. Eq. (22), we can rewrite  $[g(i_0)g^+(j_0)]_{12} = z_1^*(i_0)z_2^*(j_0) - z_2^*(i_0)z_1^*(j_0)$ . Thus, we see that the tunneling term between neighboring solitons is precisely the hopping term of the  $t$ - $J$  model when it is written in terms of the slave fermions and Schwinger bosons in conjugate representations for the two sublattices. Apart from renormalizing  $t$  to  $\tilde{t}$ , the only difference is that the correlation between the hole location and the spin magnitude has been included in the mean-field calculation of the Hubbard model. This correlation has been taken into account in determining the size of the soliton.

So far, we have eliminated the high energy processes of order  $U$ . The new “elementary particle” is the soliton. The effective action at this level consists of Eq. (44) and (B39) which are equivalent to the  $t$ - $J$  model (43). The remaining energy scales are  $t$  (we redenote  $\tilde{t}$  by  $t$ ) and  $J$ . In the next step, we want to construct the quasiparticle from the soliton and eliminate the energy scale  $t$ . Two of the present authors have recently shown how to construct a quasiparticle state in the Néel state and calculated the quasiparticle dispersion and spectral weight.<sup>20</sup> When the Néel order is destroyed by finite doping, we shall construct the quasiparticle state from a smoothly varying antiferromagnetic background. The spirit is the adiabatic approximation: The hopping of the solitons is a local and high-energy process while the low-energy spin excitations are described by slow variation of the spin directions. Without holes, the short wavelength spin fluctuations cost a lot of energy and can be eliminated. The result is the renormalization of the coefficients in the non-linear sigma model. In the doped case, the energy cost of short wavelength spin fluctuations near the solitons is compensated by the energy gain resulting from the hopping of the solitons. Therefore, short wavelength spin fluctuations cannot simply be eliminated as in the undoped case.

Let  $|SRO\rangle$  be a typical spin configuration in a short range antiferromagnetically correlated state in an arbitrary region of space, this configuration can be obtained from the perfectly ordered state by applying smoothly varying SU(2) rotations:

$$|SRO\rangle = \prod_i g(i)|SDW\rangle. \quad (\text{B40})$$

We apply the soliton creation operator to this configuration to generate a soliton at an arbitrary site

$$|i_0, l = 0\rangle = f_{i_0}^\dagger |SRO\rangle, \quad (\text{B41})$$

where we used the notation  $l = 0$  to indicate that the number of highly frustrated spins is zero, i.e. there is no spin which is almost parallel to its neighboring spins. Applying on  $|i_0, l = 0\rangle$  the effective Hamiltonian for the solitons, i.e. the  $t$ - $J$  Hamiltonian (43), a new state  $|i_0, l = 1\rangle$  is generated,

$$H_{t-J}|i_0, l = 0\rangle = -2t|i_0, l = 1\rangle + \langle i_0, l = 0|H_{t-J}|i_0, l = 0\rangle |i_0, l = 0\rangle + \dots, \quad (\text{B42})$$

where  $|i_0, l = 1\rangle$  is generated by the hopping term of the  $t$ - $J$  model. It is a superposition of four configurations in which the soliton has made one hop from the original site  $i_0$  to anyone of the four neighbors. The notation  $l = 1$  indicates that there is one spin, at the site  $i_0$ , which is frustrated with its neighbors. This is the generalization of the string state of one unit length discussed in Ref. 20 to the smoothly varying antiferromagnetic background. The other generalized string states,  $|i_0, l\rangle$  for  $l \geq 1$ , are constructed by repeatedly applying the  $t$ - $J$  Hamiltonian to  $|i_0, l = 1\rangle$ .

$$H_{t-J}|i_0, l = 1\rangle = -2t|i_0, l = 0\rangle - \sqrt{3}t|i_0, l = 2\rangle + \langle i_0, l = 1|H_{t-J}|i_0, l = 1\rangle |i_0, l = 1\rangle + \dots, \quad (\text{B43})$$

$$H_{t-J}|i_0, l\rangle = -\sqrt{3}t(|i_0, l - 1\rangle + |i_0, l + 1\rangle) + \langle i_0, l|H_{t-J}|i_0, l\rangle |i_0, l\rangle + \dots, \quad l \geq 2. \quad (\text{B44})$$

Eqs. (B42), (B43) and (B44) are the effective representation of the  $t$ - $J$  model in the determination of the quasiparticle structure. Diagonalizing these equations with appropriate  $\langle i_0, l|H_{t-J}|i_0, l\rangle$  gives rise to a quasiparticle at the site  $i_0$  of the form,

$$|i_0\rangle = \sum_{l=0}^{\infty} u_l |i_0, l\rangle, \quad (\text{B45})$$

where  $u_l$  are numerical coefficients which decrease exponentially as  $l$  increases. The quasiparticles located at other lattice sites are constructed in the same way.

The formation of the quasiparticle further renormalizes the coefficients in the non-linear sigma model. Although it is not easy to calculate the renormalization accurately, it is rather easy to see that hole (or soliton) hopping inside the quasiparticle reduces the spin stiffness. The spin stiffness is roughly proportional to the longitudinal spin magnitude. The soliton hopping inside the quasiparticle reduces the average spin magnitude  $\langle S \rangle$  by an amount of  $(2\langle l \rangle \langle S \rangle + 1)$

times the density of holes, where  $\langle l \rangle$  is the average string length inside the quasiparticle, Eq. (B45). For  $J/t < 1$ , we have  $\langle l \rangle > 1$ .

Now, we show that the hopping amplitude of the quasiparticle constructed in the way described above contains a Berry phase factor. Let  $|i\rangle$  and  $|j\rangle$  be two quasiparticle states at two different sites of the same sublattice,  $i - j = x + y$  or  $2x$ , we want to show that the quasiparticle hopping amplitude in the tight-binding approximation contains the appropriate phase factor, i.e.,

$$\langle i|H_{t-J}|j\rangle - \langle i|H_{t-J}|i\rangle\langle i|j\rangle = \alpha(i-j)\langle \vec{n}_i|\vec{n}_j\rangle, \quad (\text{B46})$$

where  $\alpha(r)$  is a real coefficient, and  $|\vec{n}_j\rangle$  is the coherent spin state defined through  $\vec{n} \cdot \vec{S}|\vec{n}\rangle = S|\vec{n}\rangle$ . Since the quasiparticle hopping is generated by the quantum spin fluctuations, it suffices to show that the matrix element of the Heisenberg operator  $\langle i|H_J|j\rangle$  contains the appropriate phase factor. Using Eq. (B45), we write

$$\langle i|H_J|j\rangle = \sum_{l,l'} u_l u_{l'} \langle i,l|H_J|j,l'\rangle. \quad (\text{B47})$$

The state  $|j,l'\rangle$  is a superposition of spin configurations; Each of them contains a string of length  $l'$ . So the matrix element  $\langle i,l|H_J|j,l'\rangle$  is a sum of matrix elements of  $H_J$  between two string configurations. We need to show that the matrix element of  $H_J$  between any two string configurations contain the phase factor  $\langle \vec{n}_i|\vec{n}_j\rangle$ . In the Bethe lattice approximation (without winding path), the spin exchange operator in  $H_J$  generates quasiparticle hopping by chopping off the strings in  $|j,l'\rangle$  by two units.<sup>20</sup> In all these processes, we can explicitly verify that  $\langle i,l|H_J|j,l'\rangle \propto \langle \vec{n}_i|\vec{n}_j\rangle$ . A general example is shown in Fig. 13. The existence of winding paths (Trugman process) leads to additional contributions to the matrix elements  $\langle i,l|H_J|j,l'\rangle$ . In general, these contributions are not exactly proportional to  $\langle \vec{n}_i|\vec{n}_j\rangle$ . An example is shown in Fig. 14. Although not exact, the phase factor is approximately proportional to  $\langle \vec{n}_i|\vec{n}_j\rangle$ , for smoothly varying spin directions. Furthermore, the Trugman process occurs only for  $l + l' \geq 6$  and therefore it is multiplied by a small coefficient  $u_l u_{l'}$ . Thus, we have shown that the quasiparticle hopping amplitude acquires the Berry phase factor if the spin directions vary smoothly in space and time. The Berry phase factor can be expressed in terms of the SU(2) matrices  $g(i)$ . Depending on which sublattice  $i$  and  $j$  belong to, the Berry phase factor  $\langle \vec{n}_i|\vec{n}_j\rangle$  is either  $[g(i)g^+(j)]_{11}$  or  $[g(i)g^+(j)]_{22}$ . For the quasiparticle hopping between different sublattices,  $i - j = 2x + y$  or  $3x$ , the appropriate phase factor of the hopping amplitude can be determined in the same way.

<sup>1</sup> N. F. Mott, *Metal-Insulator Transitions*, Taylor & Francis, London 1974.

<sup>2</sup> J. C. Slater, Phys. Rev. **82**, 538 (1951).

<sup>3</sup> M. Ogata and H. Shiba, Phys. Rev. **B41**, 2326 (1990).

<sup>4</sup> P. A. Lee, in *High Temperature Superconductivity Proceedings*, The Los Alamos Symposium-1989, pp.96, Ed. K. S. Bedell, D. Coffey, D. E. Meltzer, D. Pines and J. R. Schrieffer, (Addison-Wesley, Redwood City 1990).

<sup>5</sup> J. R. Schrieffer, X. G. Wen, and S. C. Zhang, Phys. Rev. Lett. **60**, 944 (1988).

<sup>6</sup> W. P. Su, Phys. Rev. **B37**, 9904 (1988). W. P. Su and X. Y. Chen, Phys. Rev. **B38**, 8879 (1988).

<sup>7</sup> H. Y. Choi and E. J. Mele, Phys. Rev. **B38**, 4540 (1988).

<sup>8</sup> E. Dagotto, Rev. Mod. Phys. **66**, 763 (1994), and references therein.

<sup>9</sup> E. Dagotto, R. Joynt, A. Moreo, S. Bacci and E. Gagliano, Phys. Rev. **B41**, 9049 (1990).

<sup>10</sup> D. Poilblanc, T. Ziman, H. J. Schulz, and E. Dagotto, Phys. Rev. **B47**, 14267 (1993).

<sup>11</sup> R. Eder and Y. Ohta, Phys. Rev. **B50**, 10043 (1994).

<sup>12</sup> S. Haas, A. Moreo, and E. Dagotto, Phys. Rev. Lett. **74**, 4281 (1995).

<sup>13</sup> A. Moreo, S. Haas, A. Sandvik, and E. Dagotto, Phys. Rev. **B51**, 12045 (1995).

<sup>14</sup> D. B. Tanner and T. Timusk, in *Physical Properties of High Temperature Superconductors*, Vol. III, edited by D. M. Ginsberg, p363, (World Scientific, Singapore, 1992).

<sup>15</sup> G. A. Thomas, D. H. Rapkine, S. L. Cooper, S. W. Cheong, A. S. Cooper, L. F. Schneemeyer, and J. V. Waszczak, Phys. Rev. **B45**, 2474 (1992). G. A. Thomas, D. H. Rapkine, S. A. Carter, T. F. Rosenbaum, P. Metcalf, and D. F. Honig, J. Low Temp. Phys. **95**, 33 (1994).

<sup>16</sup> A. J. Heeger, S. Kivelson, J. R. Schrieffer, and W.-P. Su, Rev. Mod. Phys. **60**, 781 (1988).

<sup>17</sup> W. P. Su, J. R. Schrieffer and A. J. Heeger, Phys. Rev. Lett. **42**, 1698 (1979).

<sup>18</sup> I. Affleck, in *Les Houches, Session XLIX*, edited by E. Brézin and J. Zinn-Justin, (Elsevier Science Publisher B.V., 1989).

<sup>19</sup> B. Keimer, N. Belk, R. J. Birgeneau, A. Cassanho, C. Y. Chen, M. Greven, M. A. Kastner, A. Aharony, Y. Endoh, R. W. Erwin and G. Shirane, Phys. Rev. **B46**, 14034 (1992).

- <sup>20</sup> Junwu Gan and Per Hedegård, cond-mat/9507067, to appear in Phys. Rev. B.
- <sup>21</sup> N. Bulut, D. J. Scalapino and S. R. White, Phys. Rev. Lett. **72**, 705 (1994); Phys. Rev. **B50**, 7215 (1994).
- <sup>22</sup> R. Preuss, W. von der Linden, and W. Hanke, Phys. Rev. Lett. **75**, 1344 (1995).
- <sup>23</sup> S. A. Trugman, Phys. Rev. Lett. **65**, 500 (1990).
- <sup>24</sup> Z. Liu and E. Manousakis, Phys. Rev. **B45**, 2425 (1992); Phys. Rev. **B51**, 3156 (1995).
- <sup>25</sup> E. Dagotto, A. Nazarenko, and M. Boninsegni, Phys. Rev. Lett. **73**, 728 (1994).
- <sup>26</sup> R. Putz, R. Preuss, and A. Muramatsu, cond-mat/9410039.
- <sup>27</sup> P. B. Weigmann, Phys. Rev. Lett. **60**, 821 (1988).
- <sup>28</sup> R. Shankar, Phys. Rev. Lett. **63**, 203 (1989).
- <sup>29</sup> X. G. Wen, Phys. Rev. **B39**, 7223 (1989).
- <sup>30</sup> P. A. Lee, Phys. Rev. Lett. **63**, 680 (1989).
- <sup>31</sup> A. M. Finkel'stein, Sov. Sci. Rev. A. Phys. **14**, 1 (1990). See e.g. Eq. (2.9).
- <sup>32</sup> H. Schulz, Phys. Rev. Lett. **65**, 2462 (1990).
- <sup>33</sup> At half-filling, the Hubbard gap in one dimension should be proportional to  $\exp(-2\pi t/U)$  for  $U/t \ll 1$ . This is equivalent to have the correct weak-coupling scaling equation. The factorization of the Hubbard interaction in terms of the vector spin field in Reference 36 results in a Hubbard gap that is exponentially wrong, as noted by Schulz<sup>32</sup>.
- <sup>34</sup> F. D. M. Haldane, Phys. Lett. **A93**, 464 (1983); Phys. Rev. Lett. **50**, 1153 (1983).
- <sup>35</sup> H. Levine, S. B. Libby and A. M. M. Pruisken, Phys. Rev. Lett. **51**, 1915 (1983).
- <sup>36</sup> N. Nagaosa and M. Oshikawa, cond-mat/9412003.
- <sup>37</sup> M. Takayama, Y. R. Lin-Liu and K. Maki, Phys. Rev. **B21**, 2388 (1980).
- <sup>38</sup> S. Kivelson, Ting-Kuo Lee, Y. R. Lin-Liu, Ingo Peschel, and Yu Lu, Phys. Rev. **B25**, 4173 (1982).
- <sup>39</sup> See e.g. V. J. Emery, in *Highly Conducting One-dimensional Solids*, edited by J. T. Devrese, R. P. Evrard, and V. E. Van Doren, (Plenum Press, New York 1979).
- <sup>40</sup> P. W. Anderson, Science **235**, 1196 (1987).
- <sup>41</sup> F. C. Zhang and T. M. Rice, Phys. Rev. **B37**, 3759 (1988).
- <sup>42</sup> S. Chakravarty, B. I. Halperin, and D. R. Nelson, Phys. Rev. **B39**, 2344 (1989).
- <sup>43</sup> T. Dombre and N. Read, Phys. Rev. **B38**, 7181 (1988). X. G. Wen and A. Zee, Phys. Rev. Lett. **61**, 1025 (1988). F. D. M. Haldane, Phys. Rev. Lett. **61**, 1029 (1988). E. Fradkin and M. Stone, Phys. Rev. **B38**, 7215 (1988).
- <sup>44</sup> H. Shultz, Phys. Rev. Lett. **64**, 1445 (1990).
- <sup>45</sup> R. Eder, Y. Ohta, and T. Shimozato, Phys. Rev. **B50**, 3350 (1994).
- <sup>46</sup> D. M. King, Z. X. Shen, D. S. Dessau, D. S. Marshall, C. H. Park, W. E. Spicer, J. L. Peng, Z. Y. Li, and R. L. Greene, Phys. Rev. Lett. **73**, 3298 (1994). Z. X. Shen, W. E. Spicer, D. M. King, D. S. Dessau, B. O. Wells, Science **267**, 343 (1995).
- <sup>47</sup> K. Gofron, J. C. Campuzano, A. A. Abrikosov, M. Lindroos, A. Bansil, H. Ding, D. Koelling, and B. Dabrowski, Phys. Rev. Lett. **73**, 3302 (1994).
- <sup>48</sup> P. Aebi, J. Osterwalder, P. Schwaller, L. Schlapbach, M. Shimoda, T. Mochiku, and K. Kadowaki, Phys. Rev. Lett. **72**, 2757 (1994).
- <sup>49</sup> I. Affleck, in *Physics, Geometry, and Topology*, page 1, edited by H. C. Lee, (Plenum Press, New York 1990).

FIG. 1. Cartoon picture of the quasiparticles, represented by the small spheres, surfing on the fluctuating membrane whose normal directions define the local directions of the magnetic moments. The north pole of the spheres represents the quasiparticle spin direction which must be perpendicular to the membrane. The normal vectors of the membrane form a sphere of unit radius. The quasiparticle traveling a closed path picks up a phase that is proportional to the area in the unit sphere enclosed by the normal vectors of the membrane along the quasiparticle trace.

FIG. 2. Hartree-Fock solution of a holon in a 100-site chain with open boundary condition for  $U/t = 8/3$ . The zigzag of the spin density near the two ends of the chain is due to the open boundary condition and has no influence on the holon solution at the middle of the chain.

FIG. 3. The one-electron spectrum of the Hamiltonian (26) for  $U/t = 8/3$ . For clarity the whole spectrum has shifted up by amount 0.148, i.e. taking  $\tilde{\mu} = \mu - U/2 = -0.148$  in Hamiltonian (26). There are two localized states inside the Mott-Hubbard gap. Each localized state contains 50% spectral weight transferred from each of the two Hubbard bands.

FIG. 4. The wave functions of the midgap localized states of the one-electron spectrum around the holon for  $U/t = 8/3$ . The lines are the guide to the eye.

FIG. 5. Fitting the spin and charge densities of a holon to analytic functions for  $U/t = 8/3$ . The points are the numerical solution. The lines are  $\langle n_i \rangle = 1 - 1/(2\xi_c \cosh^2[(i - i_0)/\xi_c])$  with  $\xi_c = 3.209$  for the charge density, and  $2(-1)^i \langle S_i^z \rangle = 0.545 \tanh[(i - i_0)/\xi_s]$  with  $\xi_s = 2.978$  for the spin density.

FIG. 6. The magnetization profile around the kink of optimal size for  $U/t = 8/3$ . The length of the arrows is proportional to the spin expectation value  $\langle S_i^z \rangle$ .

FIG. 7. The coarse grained magnetization profile of a holon. The length of the arrows is proportional to the spin expectation value  $\langle (S_i^z + S_{i+1}^z)/2 \rangle$ , and the arrows are placed at the middle of the lattice links. After coarse graining, the magnetizations are nonzero only around the kink and they sum to zero. Thus, the holon carries  $S^z = 0$ .

FIG. 8. Variational energy of the kink when an additional electron is filled into the midgap states for  $U/t = 8/3$ . The kink as a local deformation becomes unstable and decays into a smooth twist. The reference energy is that of the SDW state at half-filling of the 100-site chain with open boundary condition. The lines are the guide to the eye.

FIG. 9. Sketch of a spinon excitation which is a smooth twist of the local magnetizations.

FIG. 10. The profile of the spin and charge densities  $2(-1)^{i_x+i_y} \langle S_i^z \rangle$  and  $1 - \langle n_i \rangle$  of the spin bag solution for  $U/t = 6$  in a  $14 \times 14$  lattice with periodical boundary condition. Only the region near the bag is shown. The lattice spacing is the same as the mesh unit.

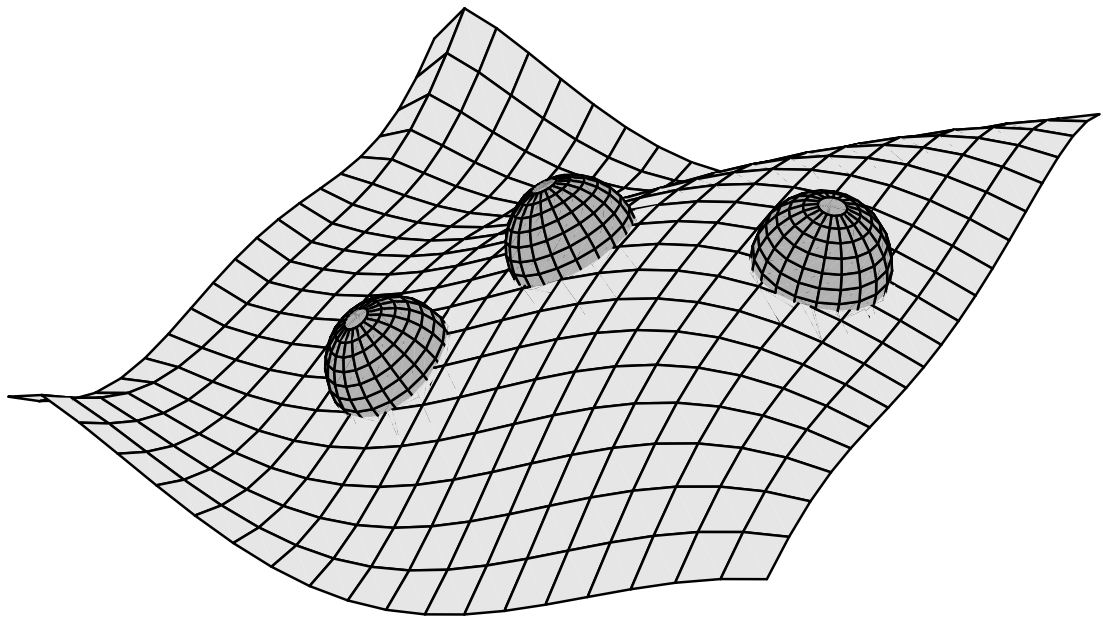
FIG. 11. The one-electron spectrum of the spin bag solution for  $U/t = 6$ . There are two localized states inside the Mott-Hubbard gap. Each midgap level can be thought of as being pushed out of one of the two Hubbard bands.

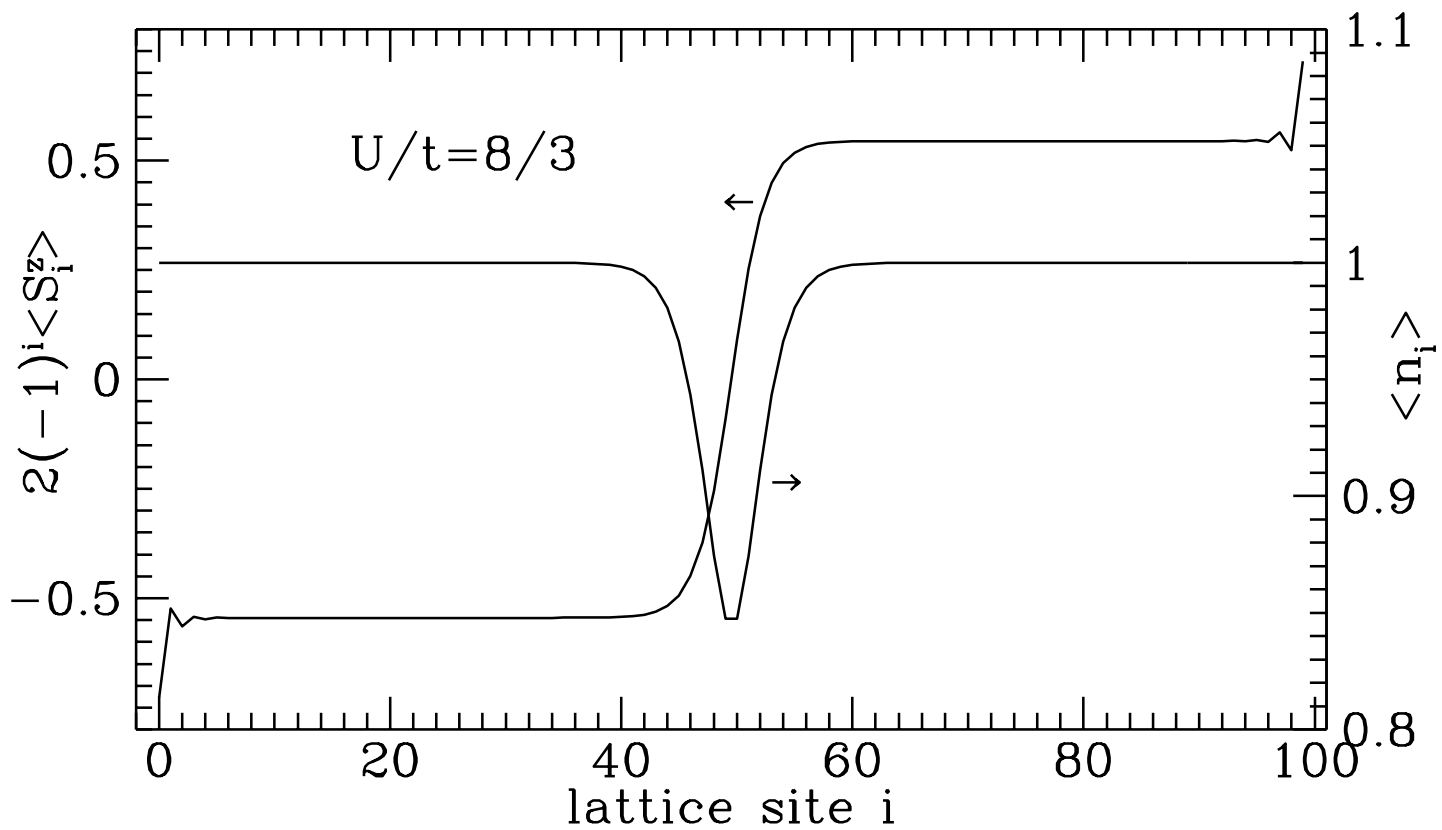
FIG. 12. The variations of the local magnetizations from the half-filled case for  $U/t = 6$ . The length of arrows is proportional to  $\delta \langle S^z \rangle$ . The length of the center arrow has been reduced by a factor of 10 for clarity. The changes are localized around the center of the spin bag, and they sum to  $\pm 1/2$ . The sign depends on which sublattice the center of the spin bag resides. Thus, the spin bag carries  $S^z = \pm 1/2$ , in contrast to the holon in 1D which carries  $S^z = 0$ . Note that the variation of the staggered magnetization has the same meaning as the coarse grained ones shown in Fig. 7 since the coarse graining at half-filling over each plaquette yields zero everywhere.

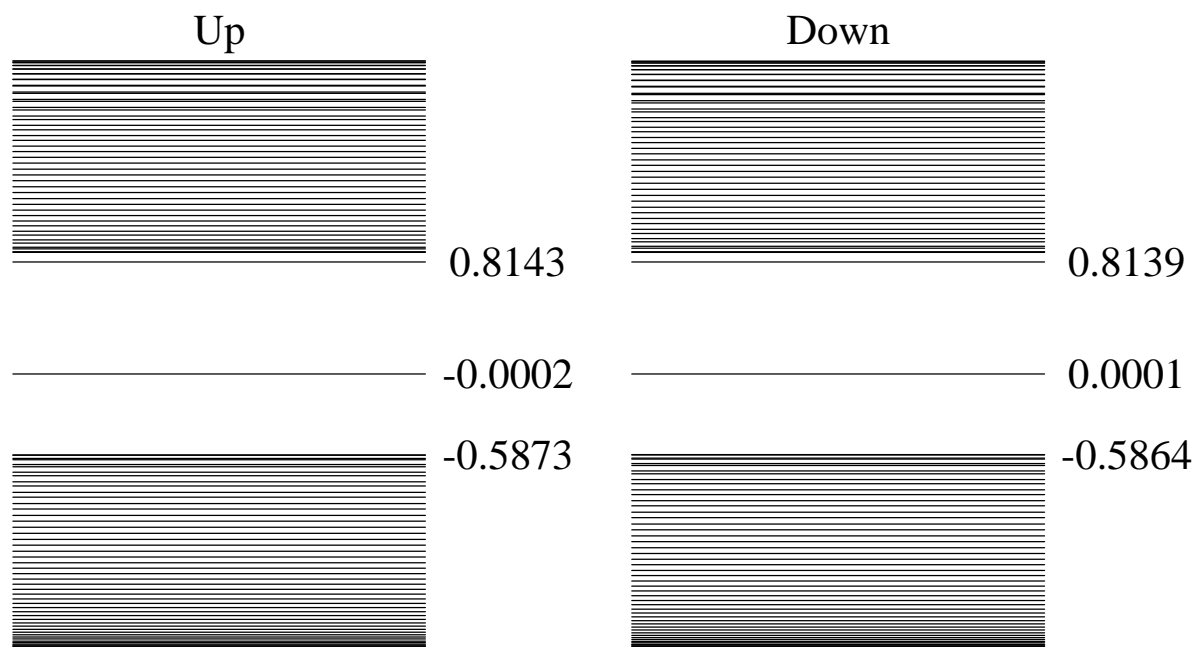
FIG. 13. A general example of the processes generating quasiparticle hopping with no winding path. Starting from configuration  $A$ , we remove a hole either at the site  $i$  or  $j$ , marked by the circles, to generate  $B$  or  $B'$ . The hole in  $B$  hops three times to generate  $C$  which contains a string of length 3 marked by the dashed line.  $C'$  is generated from  $B'$  by one hop of the hole.  $C$  and  $C'$  belong to  $|i, l = 3\rangle$  and  $|j, l' = 1\rangle$  respectively.  $H_J$  contains the spin exchange operator that can exchange the first two spins along the string in  $C$ . The resulting configuration after exchange is shown in  $D$  together with  $C'$ . The matrix element  $\langle i, l = 3 | H_J | j, l' = 1 \rangle$  is proportional to  $\langle \vec{n}_i | \vec{n}_j \rangle$ .

FIG. 14. An example of the Trugman process generating quasiparticle hopping. The configurations  $B$  and  $B'$  are generated by removing a hole in  $A$  either at the site  $a$  or  $e$ , marked by the circles.  $C$  is a configuration in  $|a, l = 6\rangle$ .  $H_J$  can exchange spins  $e$  and  $b$  in configuration  $C$ , generating  $D$ . The contribution of this example to  $\langle a, l = 6 | H_J | e, l' = 0 \rangle$  is given by the overlap between  $D$  and  $B'$ , and is proportional to  $\langle \vec{n}_a | \vec{n}_e \rangle \langle \vec{n}_c | \vec{n}_e \rangle \simeq \langle \vec{n}_a | \vec{n}_e \rangle$  in the smooth antiferromagnetic background.

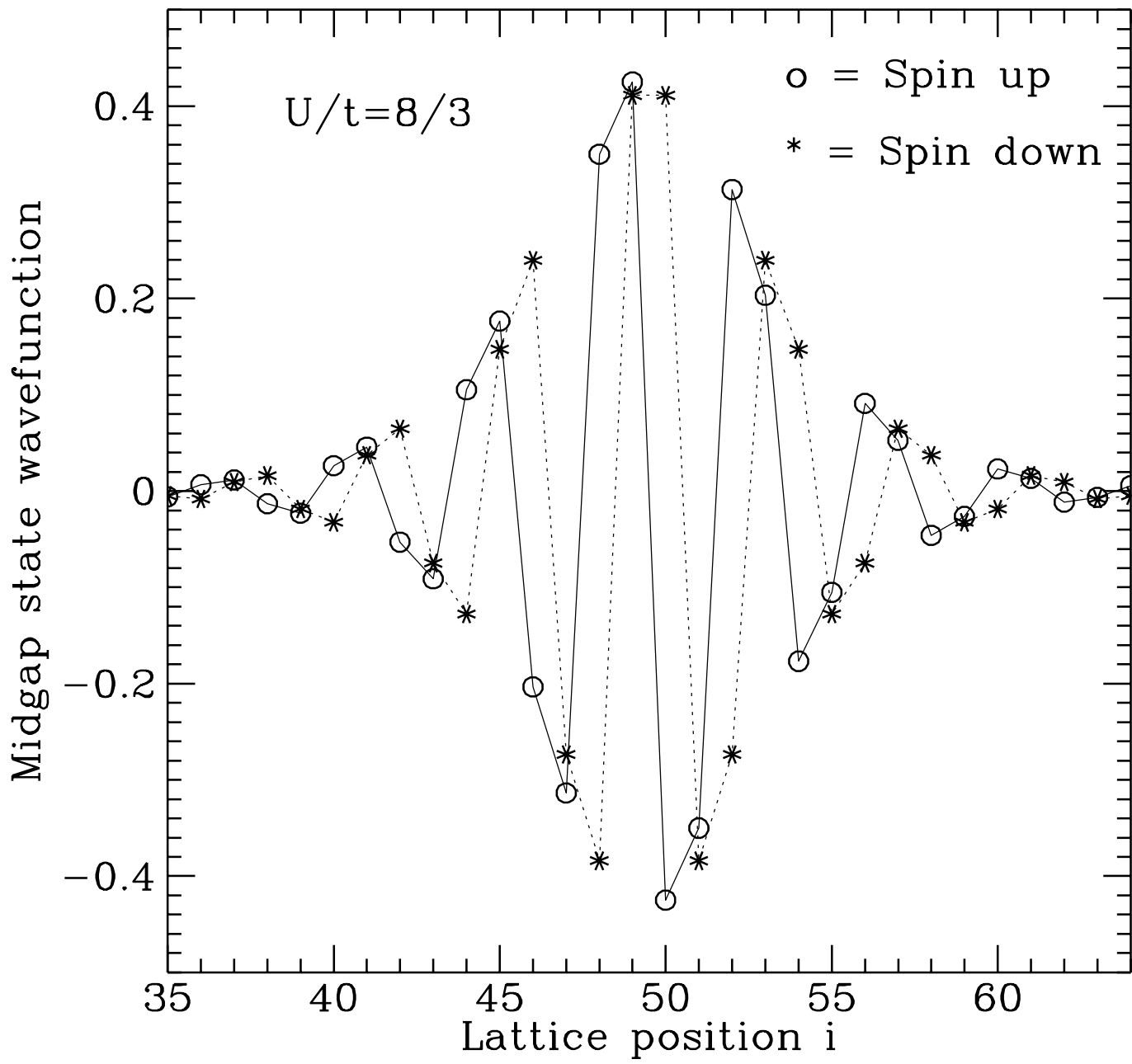


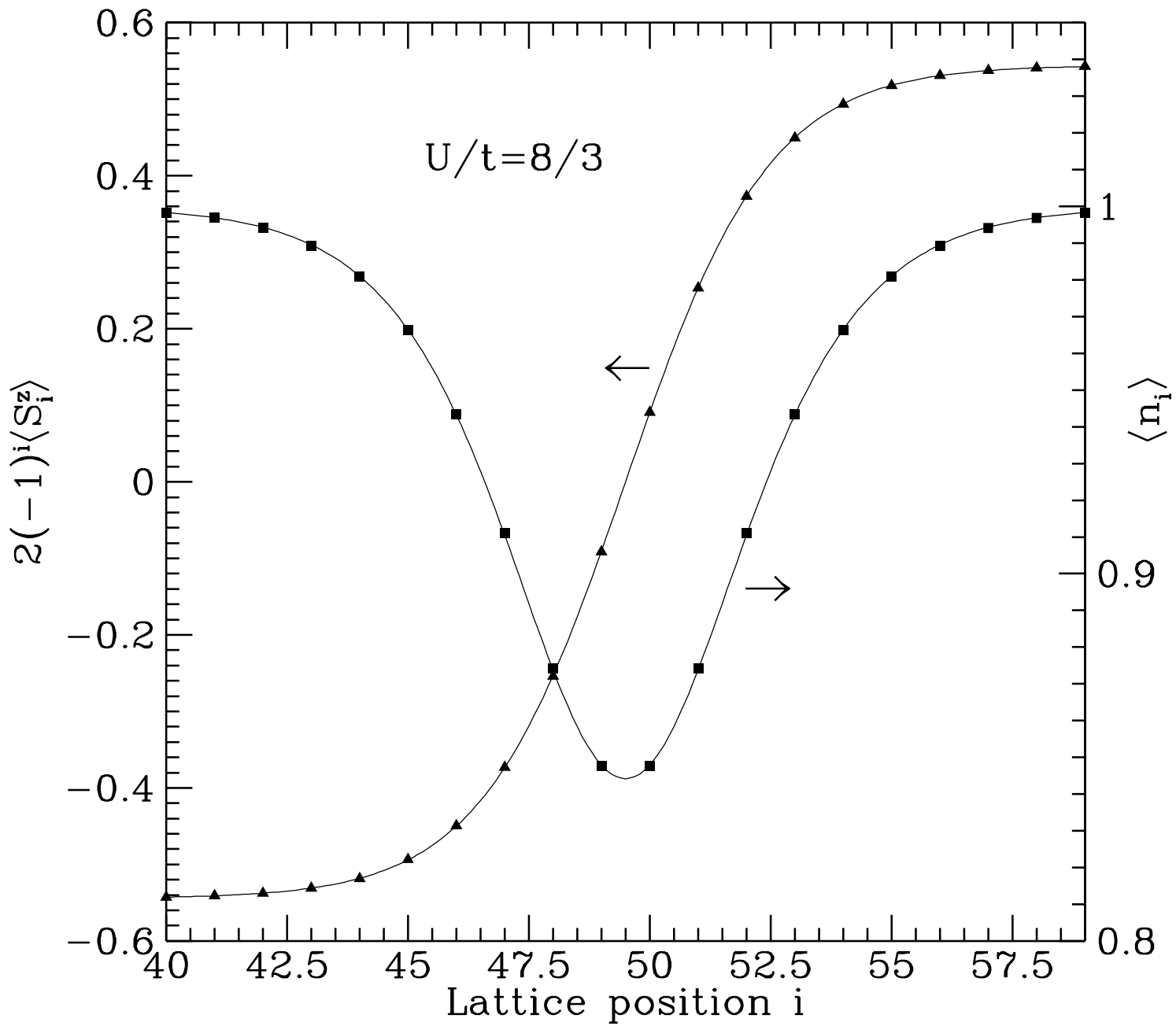




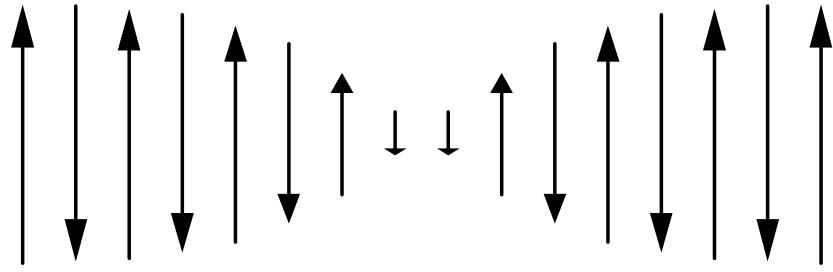


$t = 1, U = 8/3$

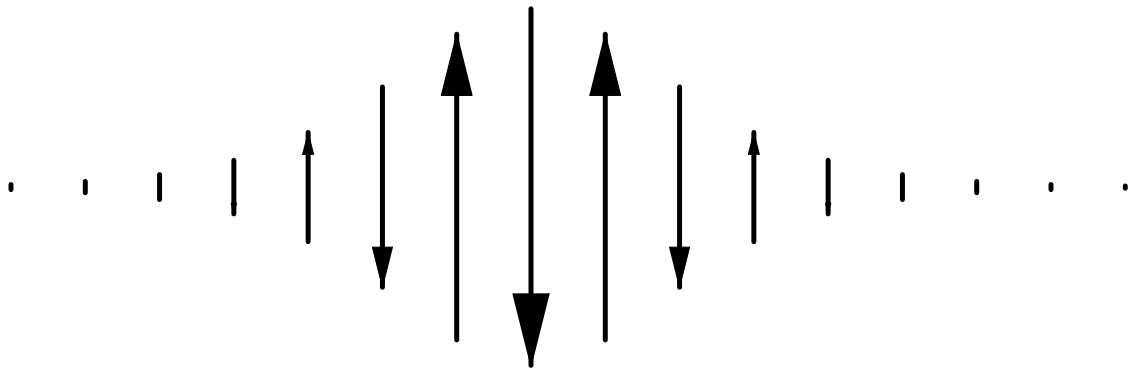


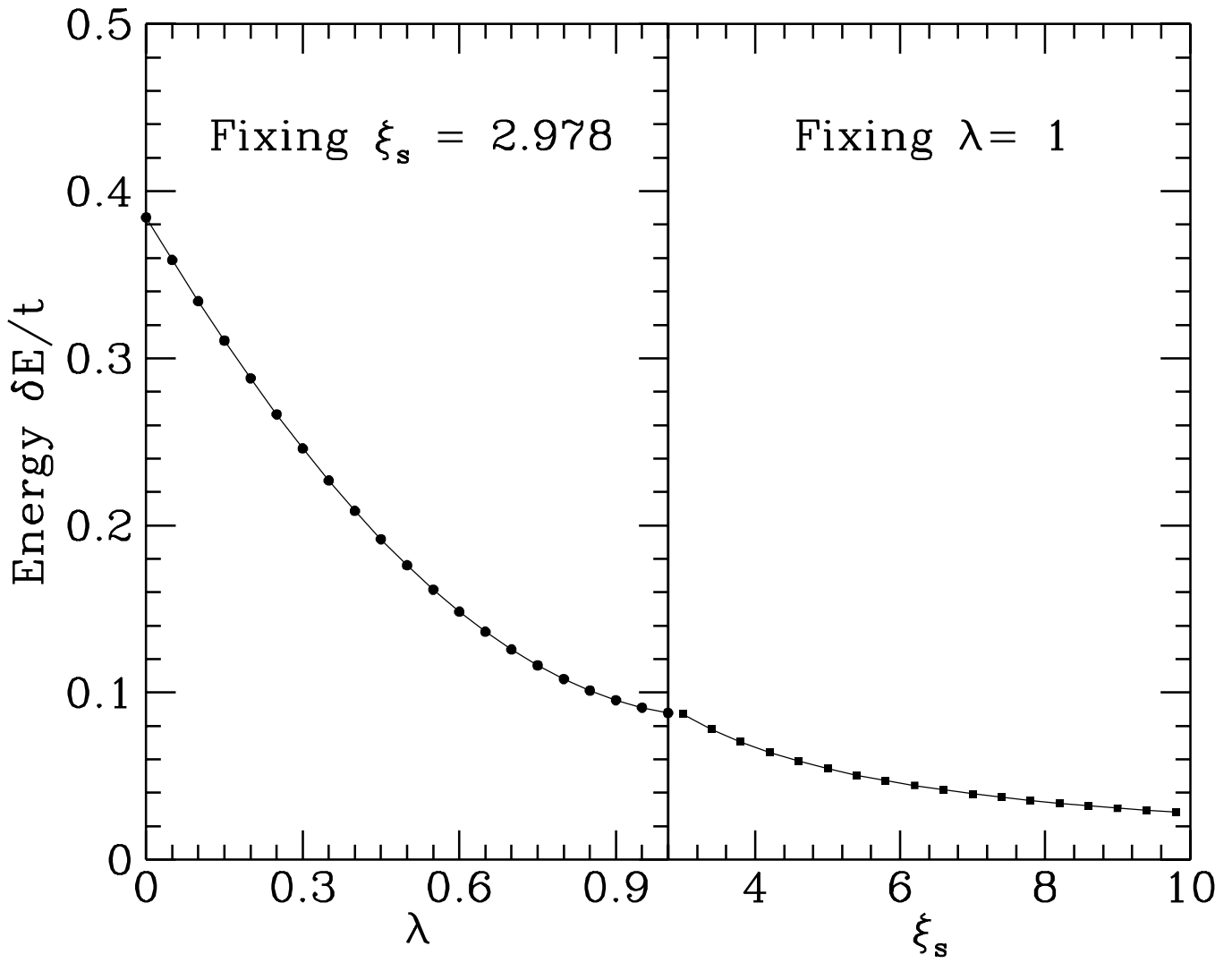


# Spin profile of a holon



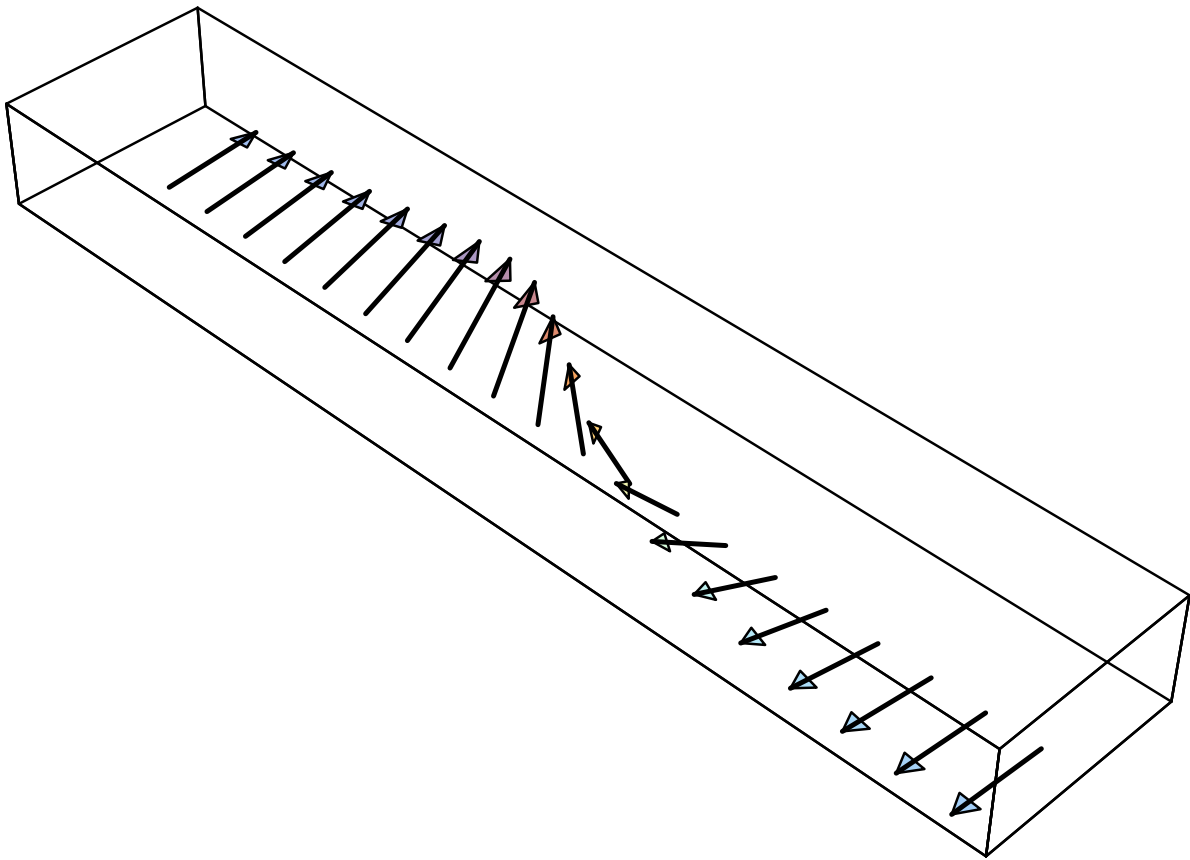
# Coarse grained spin profile of a holon



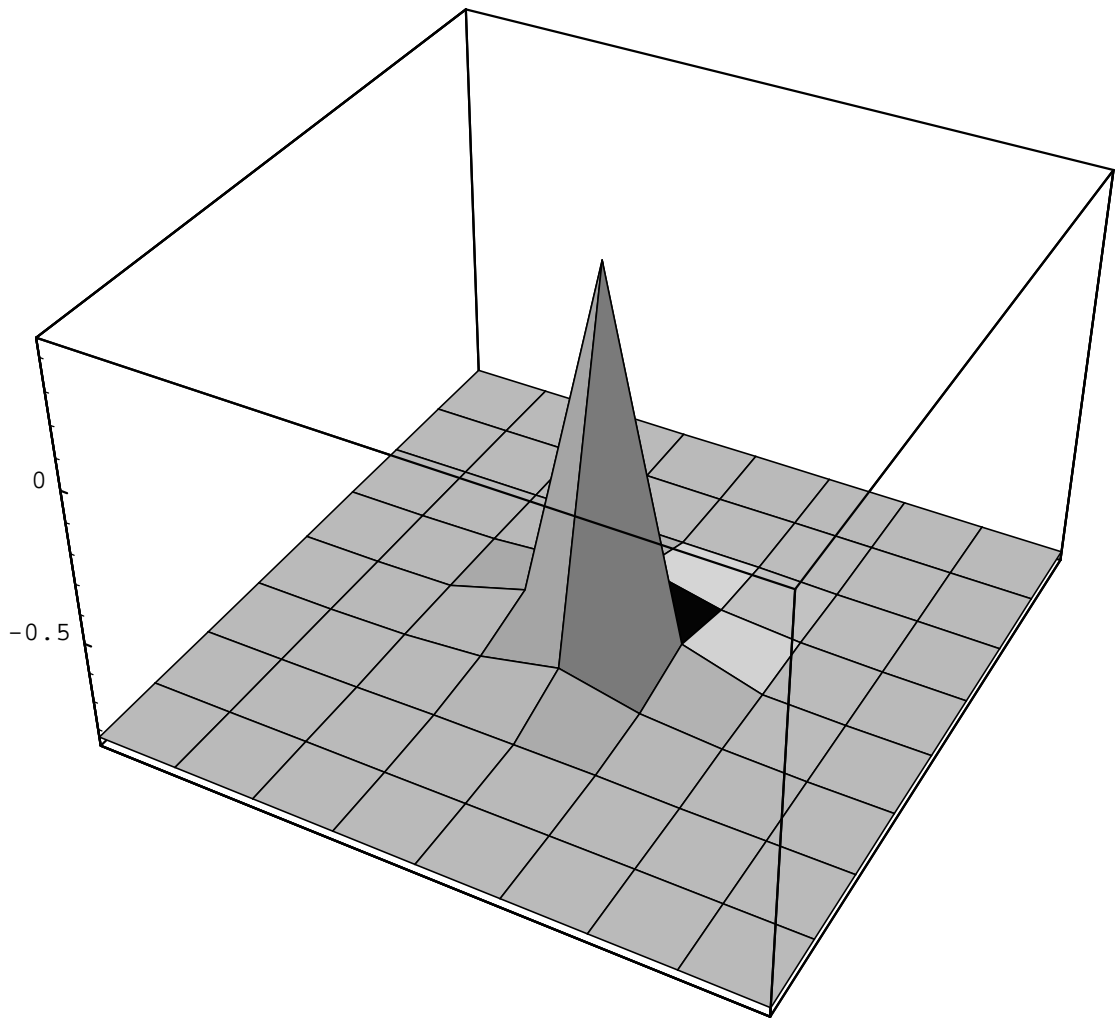




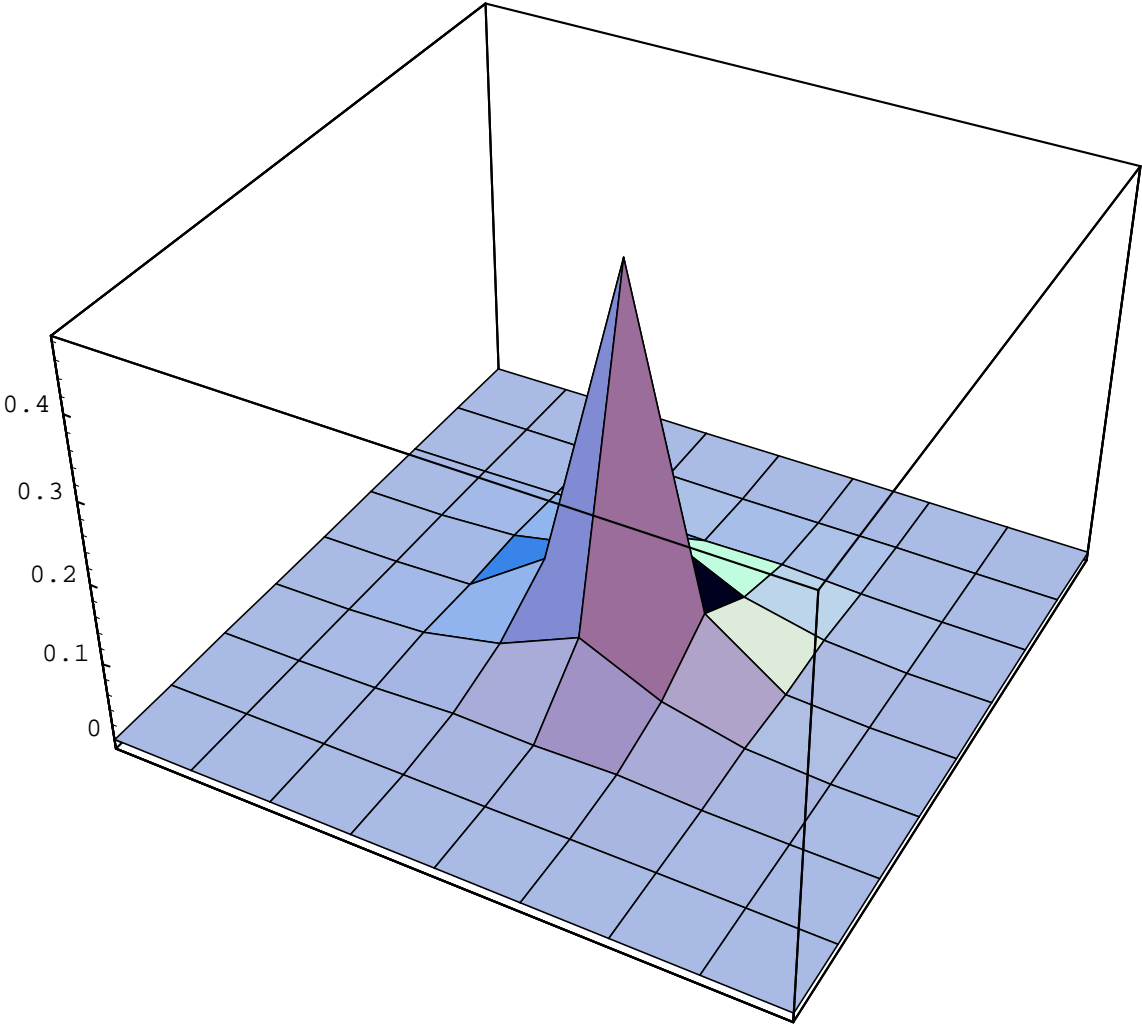
# Spin profile of a spinon



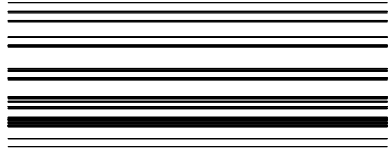
# Spin Density Variation



# Charge Density Variation

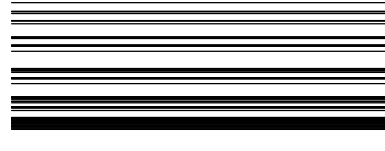


Up



2.1082

Down



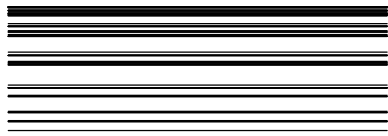
2.4172

$E = 0$

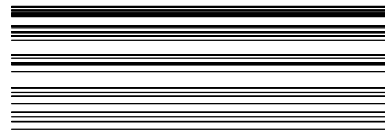


-0.9339

-1.0378

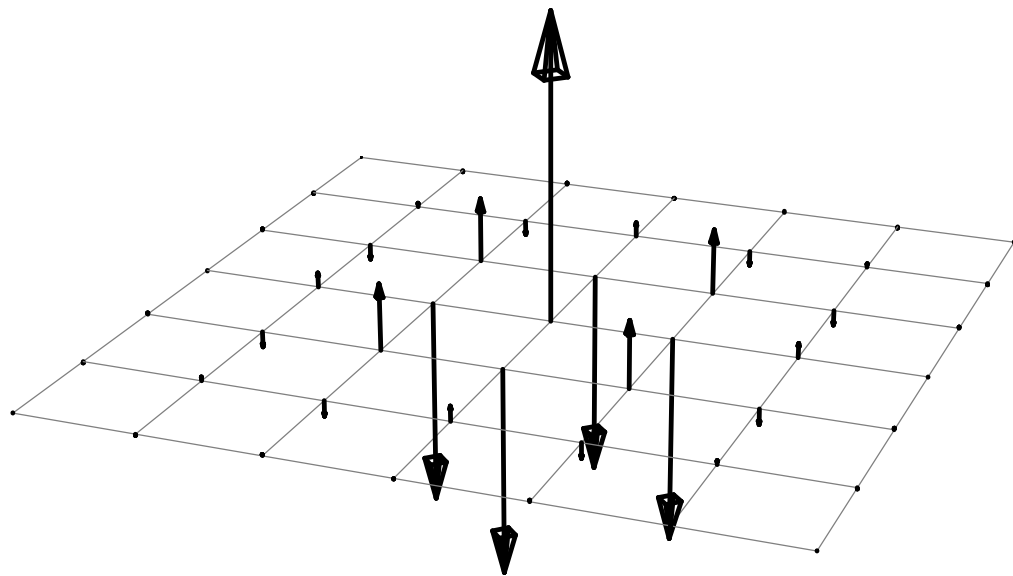


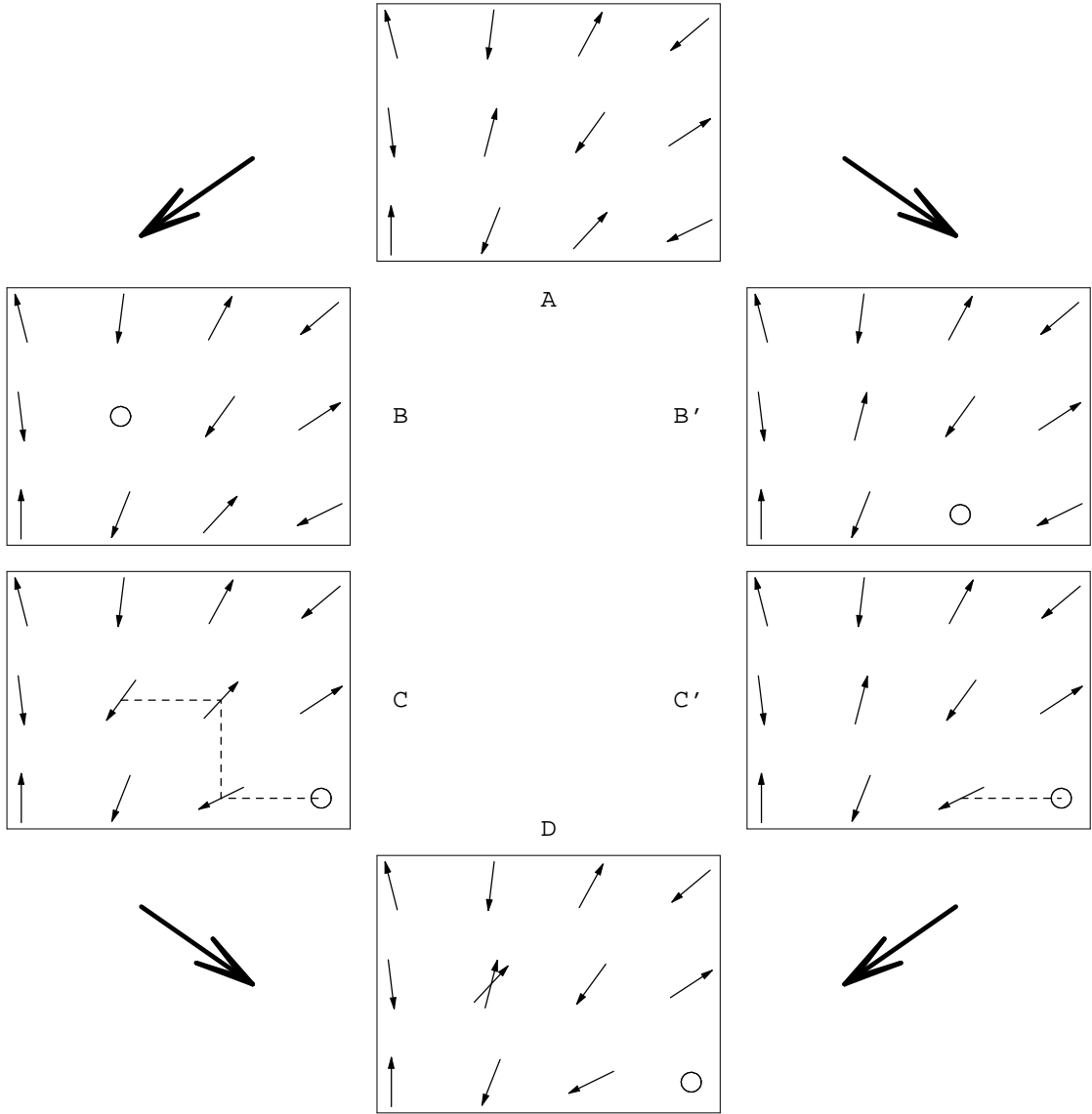
-2.4820

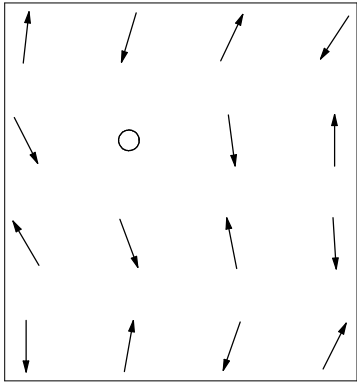
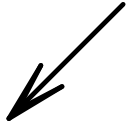
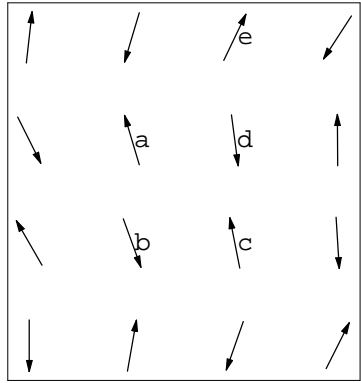


-2.4719

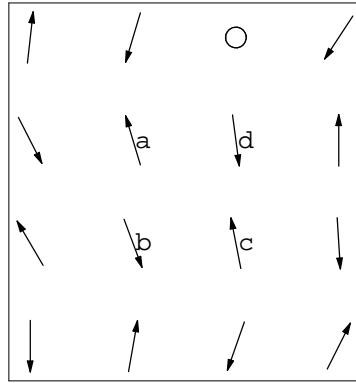
$t = 1, U = 6$



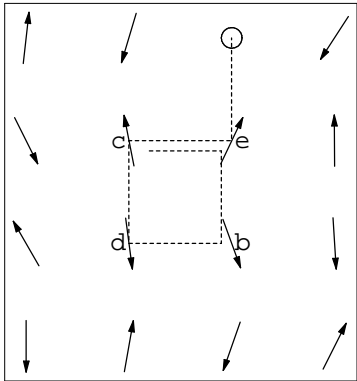




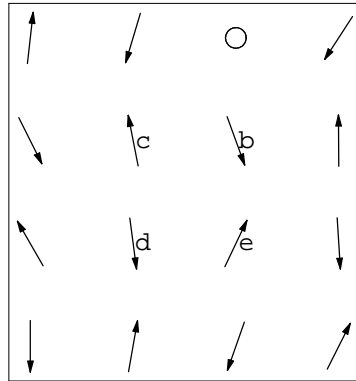
A  
B



B'



C



D